Contrib. Mineral. Petrol. 71, 343–372 (1980)

Contributions to Mineralogy and Petrology

The Colima Volcanic Complex, Mexico

I. Post-Caldera Andesites From Volcán Colima

James F. Luhr and Ian S.E. Carmichael
Dept. of Geology and Geophysics, University of California, Berkeley, California 94720, USA

Abstract. Volcán Colima is Mexico's most historically active andesitic composite volcano. It lies 150 km north of the Middle America Trench at the western end of the Mexican Volcanic Belt, closer to the trench than any other composite volcano in Mexico. Since its earliest reported eruption in 1576, V. Colima has evolved through three cycles of activity. Each cycle culminated in a major ashflow eruption, halting activity for 50 or more years. The last major ashflow eruption occurred in 1913. Andesitic block lava eruptions in 1961–1962 and 1975–1976 marked the inception of activity in a fourth historical cycle which may also terminate with a major ashflow eruption in the early part of the next century.

Major and trace element analyses of whole rock samples and all constituent phases are presented for a suite of nine post-caldera hornblende and olivine-andesites. The suite includes samples from Colima's four major eruptions since 1869, spanning the last two eruptive cycles. Colima's post-caldera andesites are poor in K and other incompatible elements (Ti, *P*, Zn, Rb, Y, Zr, Ba, La, Yb, Hf, Th, and U) as may be characteristic of near trench andesites. From the 1913 ashflow eruption through the fourth cycle andesites, there have been increases in whole rock abundances of Si, Ba, and Cs, and decreases in Ti, Fe, Mg, Ni, Cr, and Sc. Crystal fractionation models can closely reproduce major element variations in the post-caldera suite, but systematically fail to predict sufficient concentrations of the compatible trace elements Cr, Ni, and Zn. Anomalous enrichments of compatible trace elements in Colima's andesites probably reflect simultaneous crystal fractionation and magma mixing in the subvolcanic system.

Estimated pre-eruptive temperatures range from 940°–1,000° C in the hornblende-andesites and 1,030°–1,060° C in the olivine-andesites. Pre-eruptive magmatic water contents of 1.0–3.6 wt.% are calculated for the hornblende-andesites; the phenocryst assemblage of the olivine-andesite is calculated to equilibrate at 1,000 bars with 0.8% H_2O.

Orthopyroxenes and certain clinopyroxenes in all pre-1961 samples are reversely zoned, with relatively Mg-rich rims. The most pronounced Mg-rich rims occur in the olivine-andesites and are thought to reflect pre-eruptive magma mixing, involving a basic, olivine+/−clinopyroxene-bearing magma. In addition to their normally zoned pyroxenes, the post-1961, fourth cycle andesites display a number of other features which distinguish them from earlier post-caldera hornblende-andesites of similar bulk composition. These include: (1) higher total crystal contents, (2) lower modal hornblende contents, (3) higher calculated pre-eruptive silica activities, and (4) lower calculated pre-eruptive water contents. These features are all consistent with the interpretation that the fourth cycle andesites were less hydrous prior to eruption. The slight Mg-rich pyroxene rims in pre-1961 hornblende-andesites may record late-stage, pre-eruptive increases in magmatic water content, which act to raise magmatic f_{O_2} and Mg/Fe^{+2} ratios in the melt and in all crystalline phases. The fourth cycle andesites apparently did not experience a strong, pre-eruptive influx of water, resulting in lower magmatic water contents and normally zoned pyroxenes.

General Geology

Quaternary volcanism in Mexico has been primarily confined to an irregular, east-west trending belt of large andesitic composite volcanoes, intervening cinder and lava cones, and rare rhyolitic complexes which are collectively referred to as the Mexican Volcanic Belt (Mooser, 1969) (Fig. 1). The main axis of the belt is defined by a line of large, historically active composite volcanoes including Volcán Colima (4,000 m), Popocatepetl (5,452 m), and Pico de Orizaba (5,675 m) (Mooser, 1958). The easternmost, Tuxtla volcanoes, including the historically active Volcán San Martin, are

0010-7999/80/0071/0343/$06.00

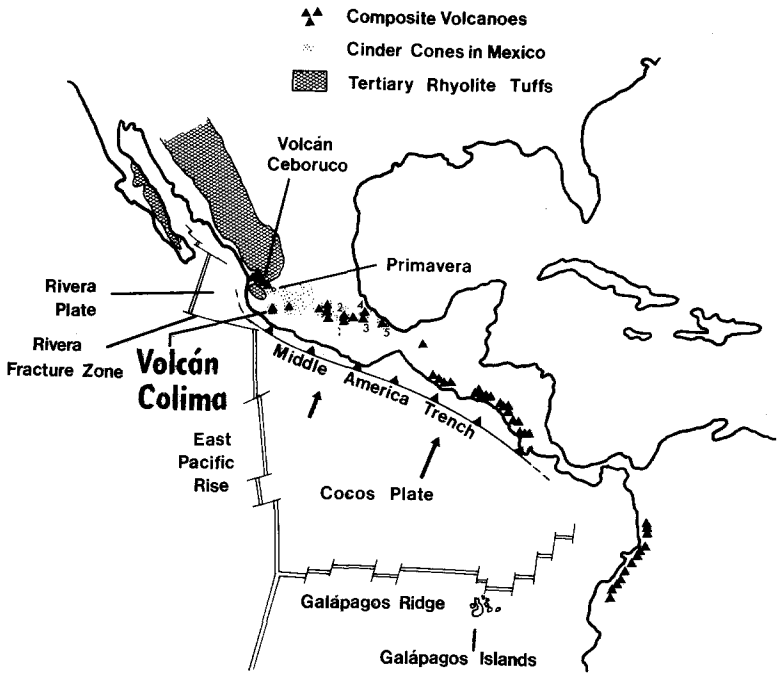

Fig. 1. Generalized map of Mexico and Central America indicating major composite volcanoes, cinder cones in Mexico, the Tertiary rhyolitic tuffs of the Sierra Madre Occidental, and principal plate tectonic features of the adjacent Pacific Ocean basin. Numbered composite volcanoes: **1**: Popocatepetl, **2**: Iztaccihuatl, **3**: Pico de Orizaba, **4**: Cofre de Perote, and **5**: Volcán San Martin

constructed of alkalic lavas ranging from picrites to hawaiites and are compositionally distinct from Mexico's other major volcanoes (Thorpe, 1977; Robin and Tournon, 1978). Cinder and lava cones are largely restricted to the basal plains surrounding composite volcanoes, but several extensive fields exist that are dominated by smaller cones. The largest such field is in the western end of the volcanic belt, northeast of Volcán Colima, and includes the historically erupted Jorullo (1759–1774; Mooser, 1958) and Paricutin (1943–1952; Foshag and Gonzalez, 1956; Williams, 1950).

Throughout the Mexican Volcanic Belt, the locations of major volcanic centers are fundamentally controlled by basement structures (Mooser, 1969, 1972). Volcán Colima lies at the southern end of the 90 km long, SSW trending Colima graben, which marks the western end of the main volcanic belt. At its northern end, some 50 km SSW of Guadalajara, the Colima graben intersects and merges with two other major structural features. The Chapala graben, containing Lake Chapala, extends 75 km east from this intersection, while a chain of small composite volcanoes trends 180 km to the northwest, parallel to the trace of the Tamayo Fracture Zone and other transform faults in the adjacent Gulf of California. This northwestern segment of the volcanic belt contains abundant alignments of cinder cones and fault scarps along northwestern trends. Gastil and Jensky (1973) present evidence for major right lateral faulting in this zone since the late Cretaceous. The late-Pleistocene Primavera complex of mildly peralkaline rhyolitic domes and pyroclastics (Mahood, 1977) lies 35 km north of the junction of these three structures.

Principal plate boundaries of the Pacific Ocean basin adjacent to Mexico include the Middle America Trench, the Galapágos Ridge, the East Pacific Rise, and the Rivera Fracture Zone (Fig. 1). These separate the oceanic crust into the Cocos and Rivera plates. The Mexican Volcanic Belt presumably developed in response to the current northeastward subduction of the Cocos Plate into the Middle America Trench. Molnar and Sykes (1969) estimated rates of convergence to be increasing to the southeast along the trench and indicated a poorly defined, northeastward dipping Benioff Zone to depths of 250 km below Mexico. Epicenters of intermediate depth earthquakes are generally restricted to the area south of the Mexican Volcanic Belt, such that few of the major composite volcanoes appear to be underlain by a seismic zone. The Middle America Trench trends approximately 110°, making an angle of about 15° with the main axis of the belt. Consequently, the more eastern volcanoes lie at progressively greater distances from the trench. This divergence may be related to increased plate convergence rates in the same direction, or as Mooser (1972) has suggested, to the controlling effect of basement structures on the locations of volcanic centers.

The Colima Volcanic Complex

The Quaternary Colima volcanic complex is roughly circular with a radius of approximately 12 km (Fig. 2). It straddles the border between the states of Jalisco and Colima, about 150 km northeast of the Middle America Trench. Molnar and Sykes (1969) delineated a crude Benioff Zone about 100 km below the complex, dipping at an angle of 30° to the northeast.

The complex consists of two overlapping composite volcanoes. The older, extinct cone of Nevado de Colima, centered at 19°33′44″ N, 103°36′31″ W, marks its highest point at 4,320 m. Nevado's peak has been extensively glaciated (Lorenzo, 1961). The younger Volcán de Colima, Mexico's most historically active volcano, is centered approximately 5.5 km south of Nevado's peak at 19°30′44″ N, 103°37′02″ W. The crater dome of Volcán Colima is presently at about 4,000 m elevation. Both Colima volcanoes possess large summit calderas as indicated on Fig. 2; each was partially filled by the later growth of a lava cone.

Immediately north of the Colima complex lies an older, dissected volcanic center (Fig. 2). Consequently, this area records a progressive trenchward shift in the focus of volcanism by some 20 km over the lifetimes of three composite volcanoes. In the eastern portion of the Mexican Volcanic Belt, the historically active volcanoes Popcatepetl and Pico de Orizaba each lie at the southern ends of N-S trending, extinct volcanic chains (White, 1952; Weyl,

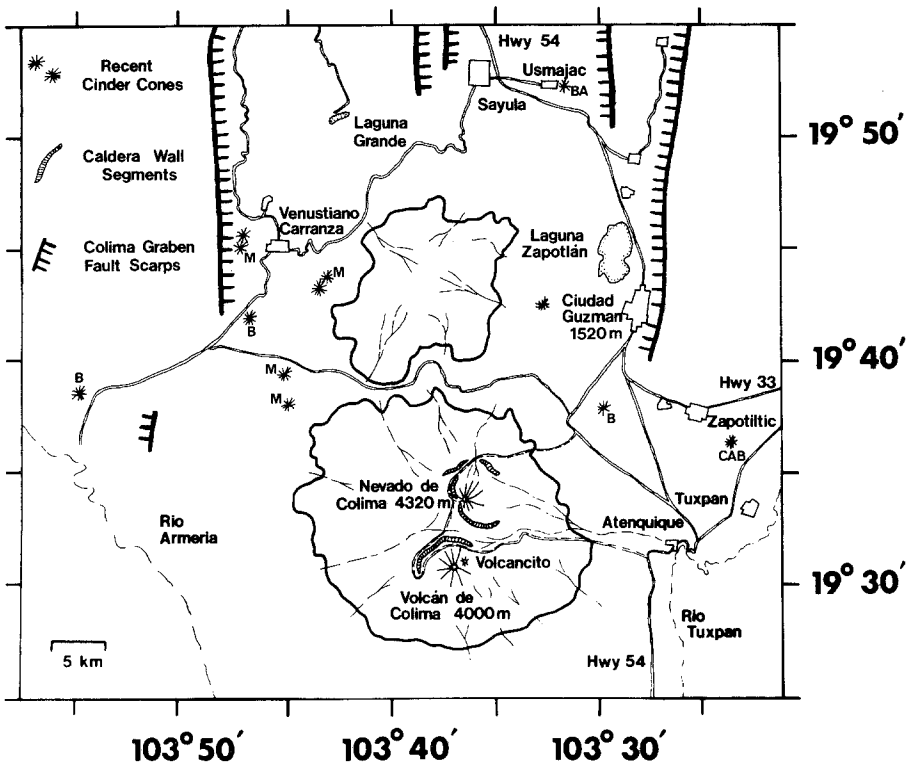

Fig. 2. Generalized map of the southern end of the Colima graben, indicating major fault scarps of the graben system, the Colima complex and the older center to the north, and surrounding cinder cones. The cinder cones are labelled *CAB* (calc-alkaline basalt), *BA* (basaltic andesite), *B* (basanite), and *M* (minette)

1974). Both of these chains also appear to have propagated trenchward with time. Similar trenchward shifts in the focus of volcanism occurred through the lives of the paired volcanoes San Pablo and San Pedro in northern Chile (Francis et al., 1974) and Nekoma and Bandai in northeastern Japan (Nakamura, 1978). In the Aleutina arc, however, Marsh (1976) noted an opposite, northward migration of volcanism with time.

A 300+ m thick apron of volcanic conglomerates, sands, and ashes drapes the base of the Colima complex and the older center to the north. The upper, gently sloping surface of this clastic apron forms a broad plain surrounding the volcanoes at about 1,500 m elevation, which becomes coincident with the floor of the Colima graben as it is followed to the north. In the valley of Rio Tuxpan, to the southeast of the complex (Fig. 2), this clastic sequence unconformably overlies a greenschist grade metavolcanic basement of unknown age at about 1,000 m elevation. Assuming that the Colima complex overlies this basement at the same elevation, its total constructional volume is estimated as 450 km^3.

Along its length, the floor of the Colima graben is alternately occupied by clastic aprons, playa lakes, and recent, small volume volcanic centers. At the southern end of the graben, a dozen or more recent cinder cones have erupted through the clastic aprons surrounding Nevado de Colima and the older volcano to the north at 900 m–1,700 m elevation (Fig. 2). Many of these cones have well preserved craters and may be only tens of thousands of years old. Nine of the cinder cones have been sampled for study. Scoria from seven of them form a transitional series from potassic basanites to minettes. The occurrence of basanites and minettes at the southern end of the Colima graben is consistent with the general association of alkalic volcanic centers and areas of extension. To our knowledge, the minettes represent the youngest and freshest known samples of lamprophyric magmas. The petrology of these cinder cones is considered in Luhr and Carmichael (1979) and in Part II of this paper.

History and Cyclicity of Eruptions From Volcán Colima

Volcán Colima is one of the most historically active volcanoes in North America. Written accounts of its eruptions date from shortly after the Spanish Conquest of Mexico, yielding a record of activity over 400 years in length. Compilations of the eruptive history of Volcán Colima were made by Barcena (1887), Sapper (1927), Friedlaender (1930), Waitz (1932), and Mooser (1958, 1961). These compilations were necessarily based on separate reports varying widely in quality and reliability. Nevertheless, it is apparent that historical activity at Volcán Colima has evolved in a highly periodic manner. Since the earliest available report in 1576, the volcano has experienced three cycles of eruptive activity. The eruption of hornblende-andesite block lava flows in 1961–1962 (Mooser and Maldonando-Koerdell, 1963) and 1975–1976 (Thorpe et al., 1977) marked the inception of activity in a fourth historical cycle.

Figure 3 is a plot of all reported eruptions of Volcán Colima[1] designated as: (1) unspecified, (2) block lava, (3) airfall ash and cinder, and (4) maximal, Pelean-type ashflow eruptions. Those eruptions whose products were sampled for study are briefly described in the next section. The last three eruptive cycles at Volcán Colima have culminated in major ashflow eruptions. Following the cycle-ending ashflow eruption of 1913, the 350 m diam. summit crater was cleared to a depth greater than 60 m (Mooser and Maldonando-Koerdell, 1959). At such times, the crater of V. Colima is probably very similar to the present, open craters of Popocatepetl and Pico de Orizaba (Mooser, 1958). The next eruptive cycle then begins with a slow, discontinuous, piston-like ascent of the lava dome in the open crater. During phases of lava dome

[1] A detailed history of eruptions is available from the authors on request

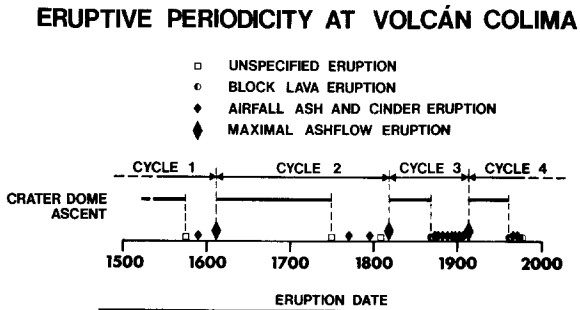

ERUPTIVE CYCLE	1	2	3	4
PRECEDING ASHFLOW ERUPTION DATE	—	1611	1818	1913
INITIAL ERUPTION DATE	1576	1749	1869	1961
FINAL ASHFLOW ERUPTION DATE	1611	1818	1913	—
DURATION OF ACTIVITY (yrs.)	35	69	44	—
DURATION OF INACTIVITY (yrs.)	—	138	51	48
DURATION OF CYCLE (yrs.)	—	207	95	—

Fig. 3. Plot of historical eruptions of *Volcán Colima* versus time and a list of data used in defining historical *eruptive cycles*. Sources of data: Barcena (1887), Sapper (1927), Friedlaender (1930), Waitz (1932), Mooser (1958, 1961), Mooser and Maldonando-Koerdell (1963), and Thorpe et al. (1977)

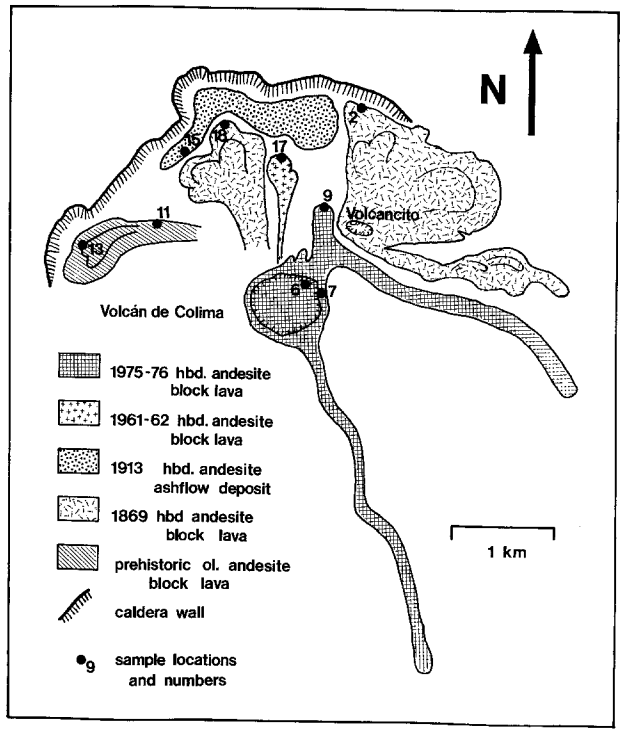

Fig. 4. Generalized map of the summit of *Volcán Colima* indicating sampled, post-caldera flows

ascent, which have lasted 50–140 years, eruptive activity is minimal to nonexistent (Fig. 3). At the termination of the dormancy phase, the dome is generally in the vicinity of the crater rim. Eruptive activity resumes in the form of pyroclastic or block lava eruptions. These phase initiating eruptions occurred in 1576, 1749, 1869, and 1961. Once begun, activity continues intermittently for 35–70 years and terminates with a maximal, ashflow dominated eruption. Cycle-ending ashflow eruptions occurred in 1611, 1818, and 1913. Following each culminating eruption, the crater dome of the next eruptive cycle begins its discontinuous ascent to the rim.

The eruptions of 1961–1962 and 1975–1976 marked the beginning of a fourth historical phase of activity at Volcán Colima. By analogy with eruptive behavior exhibited in earlier cycles, it is expected that during the next 20–50 years, pyroclastic activity will be common with lesser likelihood of further lava eruptions. The fourth cycle should end sometime in the early part of the next century with one or more large, crater-clearing ashflow eruptions. Calculations in this paper, however, point to a significant reduction in magmatic water content during the current eruptive cycle, which may lead to more subdued, less explosive behavior of the volcano.

Post-Caldera Lavas and Scoria

The active cone of Volcán Colima (4,000 m) rises 1–1.3 km above the westward sloping, infilled floor of the caldera, which itself is about 1.4 km above the surrounding Colima graben floor. The cone has overflowed and obliterated the caldera walls on all but the northern and northwestern sides (Fig. 4). Initial caldera diameter is estimated as 4.5 km; the volume of the active, post-caldera cone is approximately 5 km^3. Based on reported eruptions over the last 200 years, the average growth rate for the intracaldera cone has been approximately 0.002 km^3/yr. Extrapolation of this rate implies an age for the post-caldera cone and a minimum age for the caldera of 2,500 years.

Nine samples were collected from seven of the most recent, post-caldera andesites at Volcán Colima. Sample locations are indicated on Fig. 4 and described below in chronological order of eruption. A brief history of each sampled eruption is given when possible.

Col 11 and 13. – Several large, prehistoric flows of olivine-andesite form the floor in the northwestern part of the caldera. One of the stratigraphically oldest lobes was sampled as Col 13, and one of the youngest as Col 11. These olivine-andesites are considered to be the oldest, accessible post-caldera flows at Volcán Colima.

Col 7. – Col 7 was sampled in April, 1975, from a prominent peak on the eastern crater rim which was subsequently buried by the flows of 1975–1976. The peak is visible as the high point on the crater rim in the 1913 photograph of Waitz (1915) and in the 1961 photograph of Mooser and Maldonando-Koerdell (1963). The exact age of Col 7 is unknown, but it can confidently be placed prior to the 1869 flows in order of eruption.

Col 18 and 2. – Following the maximal ashflow eruption of February 5, 1818 (Mooser, 1961) which is interpreted as having ended the second eruptive cycle, no activity occurred at Volcán Colima for 51 years as a lava dome slowly rose in the open crater. In June of 1869, the dome was still below the crater rim, but the rising magma found an opening in the northeastern side of the main cone and the parasitic cone of Volcancito was formed about 1 km from the axis of the main crater and 100 m below its rim. Approximately 0.19 km^3 of block lava was erupted from Volcancito, filling the northeastern portion of the caldera and overflowing and obliterating the eastern caldera wall (Sartorius, 1871; Waitz, 1906; Mooser, 1961). Col 2 was collected from the northernmost flow front. Sometime after the Volcancito related flows were

erupted, the main crater overflowed its rim and a double-leveed, bilobate flow with an estimated volume of 0.08 km^3 was emplaced on the northwestern face of the cone. Sample 18 was taken from its flow front. The 1869 flows are characterized by abundant large hornblende crystals (Table 6).

Col 15. – After the major 1869 eruption, Volcán Colima experienced occassional minor and major pyroclastic eruptions until 1909 (Arreola, 1903; Sperry, 1903; Mooser, 1961), when it entered a four year period of inactivity. On January 20, 1913, a tremendous ashflow eruption began (Waitz, 1915), closing the third, historical eruptive cycle. Ash clouds from this eruption traveled to the northeast, dropping approximately 0.5 mm of ash of Guadalajara, about 140 km distant. Most of the erupted material was deposited during the first day of activity by ashflows which moved down canyons on all sides of the volcano, extending up to 8 km from the crater. The 1913 activity had a dramatic impact on the morphology of the upper cone, impressively illustrated by photographs accompanying Waitz's (1915) report. Col 15 is a scoria sample from near the base of the 7 m thick ashflow deposit forming the flat caldera floor to the north of the cone. Partial wet chemical and X-ray fluorescence analysis of the dense scoria now filling the 1869 vent of Volcancito demonstrates it to be compositionally identical to the Col 15 scoria, while distinguishable from every other analyzed sample. Since the only major, post-1869 ashflow eruption of Volcán Colima occurred in 1913, we are confident in interpreting Col 15 as a product of the cycle-ending, 1913 activity.

Col 17. – Following the tremendous ashflow eruption of 1913, the volcano was essentially dormant for 48 years, during which time a lava dome slowly rose to the crater rim. The dome stagnated in about 1935 as a flat lava plug 60 m below the rim. In May of 1957, fumarolic and solfateric activity resumed from cracks in the dome as it began arching and rising to the rim accompanied by small earth tremors (Mooser and Maldonando-Koerdell, 1959). The dome spilled over a low spot in the northern rim in mid-1961. From then until late-1962, a short block lava flow of approximately 0.02 km^3 volume descended the northern face of the cone to the caldera floor, a distance of about 300 m (Mooser and Maldonando-Koerdell, 1963). The 1961–1962 activity is interpreted as having initiated the eruptive phase of the fourth historical cycle. Col 17 was sampled from the flow front.

Col 6. – Col 6 was sampled in April, 1975 from the 13 year old crater dome prior to the 1975–1976 eruption. It is assigned an eruptive date of 1962 in this report. Stoiber (1967) investigated fumaroles and fumarolic sublimates from the crater dome of Volcán Colima in February, 1966. Sulfur, halite, sylvite, thenardite, soda alum, anhydrous sodium aluminum sulfate, and yellow iron chlorides were identified among the sublimates.

Col 9. – Between December, 1975 and June, 1976, the crater dome of Volcán Colima overflowed the northeastern and eastern crater rims. Three small lobes of blocky andesite flowed northward toward the caldera floor and two other long tongues moved down major canyons on the southeast side, reaching almost to the base of the volcano. Total eruptive volume is estimated as 0.12 km^3 The downslope movement of these lavas was accompanied by frequent block and ash-flows from the oversteepened flow fronts (Thorpe et al., 1977). Col 9 was sampled from the front of the largest, northern flow lobe in April, 1976.

Table 1. Whole rock wet chemical analyses

Col	9	6	17	15	18	2	7	11	13
SiO_2	61.02	60.41	60.41	57.57	61.09	60.84	61.61	56.55	56.46
TiO_2	0.64	0.67	0.72	0.79	0.61	0.62	0.60	0.78	0.77
Al_2O_3	17.72	18.08	17.17	17.42	17.73	17.80	17.82	16.63	16.67
Fe_2O_3	1.77	2.08	1.89	2.64	1.96	2.16	2.10	1.46	2.11
FeO	3.46	3.25	3.92	3.74	3.18	3.10	2.96	5.23	4.56
MnO	0.10	0.10	0.12	0.12	0.10	0.11	0.10	0.11	0.12
MgO	2.76	2.80	3.22	4.14	2.60	2.74	2.54	5.94	5.98
CaO	5.92	6.31	5.89	7.02	5.84	5.88	5.70	7.75	7.65
Na_2O	4.70	4.78	4.67	4.40	4.78	4.76	4.77	4.03	4.02
K_2O	1.40	1.31	1.40	1.16	1.41	1.46	1.43	1.06	1.06
P_2O_5	0.21	0.20	0.22	0.19	0.19	0.22	0.20	0.20	0.17
H_2O^+	0.06	0.09	0.13	0.49	0.07	0.10	0.10	0.15	0.18
H_2O^-	0.10	0.06	0.07	0.11	0.07	0.04	0.05	0.05	0.05
Total	99.86	100.14	99.83	99.79	99.63	99.83	99.98	99.94	99.80
CIPW norm (mol%)									
qz	10.48	9.43	9.49	6.69	10.70	10.29	11.54	3.34	4.01
or	8.25	7.69	8.26	6.86	8.33	8.60	8.42	6.21	6.23
ab	42.10	42.66	41.87	39.58	42.90	42.63	42.68	35.91	35.89
an	23.07	23.86	21.72	24.40	22.75	22.83	22.91	23.98	24.17
di	3.89	4.76	4.82	7.40	3.98	3.86	3.18	10.31	9.97
hy	9.04	8.09	10.40	10.80	8.05	8.21	7.84	17.24	16.11
mt	1.85	2.16	1.97	2.76	2.05	2.25	2.19	1.51	2.19
il	0.89	0.93	1.00	1.10	0.85	0.86	0.83	1.08	1.07
ap	0.44	0.42	0.46	0.40	0.40	0.46	0.42	0.42	0.35

Analyses by I.S.E. Carmichael
Alkalis by J. Hampel, flame photometer

Whole Rock and Groundmass Chemical Compositions

Wet chemically determined major element analyses and CIPW norms of the nine whole rock samples are listed in Table 1 in order of increasing sample age. The alkali-lime index for Colima's post caldera suite, constructed from a Harker variation diagram, is 60.6, at the calcic end of the calc-alkalic class (Peacock, 1931). This is simply a reflection of the high calcium/low alkali nature of the suite.

19 trace elements and 3 major elements determined by neutron activation analysis for 8 of the samples are listed in Table 2. 6 trace elements determined by X-ray fluorescence are tabulated for each sample in Table 3. Wet chemical and neutron activation analyses of the groundmass phase in seven of the samples are given in Tables 4 and Table 5 respectively. As is characteristic of many calc-alkaline andesites (Taylor, 1969), Colima's post-caldera andesites do not display significant Eu anomalies (Table 3). Moorbath et al. (1978) determined Sr^{87}/Sr^{86} ratios for 8 andesites and basaltic andesites from the Colima volcanoes, ranging from 0.7036–0.7040.

Calc-alkaline andesites vary widely in major element, trace element, and isotopic compositions throughout the world. Classification schemes for orogenic andesites generally rely on K_2O as a principal discriminant (Taylor, 1969), although a number of other incompatible elements may vary sympathetically with K_2O. High and low K andesites occur in both island arcs and on continental margins, with continental andesites commonly containing higher concentrations of Si and incompatible elements (Jakes and White, 1972). In many volcanic arcs, the concentrations of K_2O and related elements increase with distance from the trench (Kuno, 1959; Rittmann, 1962; Sugimura, 1968; Hatherton and Dickenson, 1969; Katsui et al., 1978). Volcán Colima lies 150 km from the Middle America Trench, closer than any other composite volcano in Mexico. Colima's investigated post-caldera andesites have relatively low concentrations of K, Ti, P, and incompatible trace elements (Zn, Rb, Y, Zr, Ba, La, Yb, Hf, Th, and U). Colima's andesites are contrasted with the incompatible element enriched post-caldera andesites from the Mexican Volcano Ceboruco (250 km from the trench) in Luhr and Nelson (1979).

Temporal Variations in Magma Composition

A number of recent studies have attempted to determine the nature and extent of variations in magma compositions with time at specific andesitic volcanoes (Condie and Swenson, 1973; Katsui et al., 1975; Ando, 1975; Rose et al., 1977; Newhall, 1978; Fairbrothers et al., 1978; Stern, 1979; Nelson, 1979; Sakuyama, 1979). While each volcano has unique aspects to its chemical evolution, most studies have documented periodic alternations between basic, intermediate, and occasionally silicic magmas superimposed on an over-

Table 2. Neutron activation analyses of whole rock samples[a]

Col	9	6	17	15	2	7	11	13
Na%	3.66	3.56	3.64	3.35	3.67	3.68	3.13	3.15
Sc	12.7	13.6	14.9	18.8	12.0	12.1	23.9	23.4
Ti%	0.31	0.38	0.36	0.40	0.32	0.31	0.41	0.37
V	150	140	196	179	169	130	229	231
Cr	25	32	35	75	34	17	210	210
Mn	811	798	900	913	833	778	991	958
Fe%	3.86	4.02	4.44	4.74	3.90	3.83	5.15	5.04
Ni	10	25	26	51	32	21	80	73
Zn	70	66	73	66	63	62	77	66
Cs	1.0	0.7	0.8	0.4	0.7	0.6	0.4	0.6
Ba	510	463	497	413	494	539	391	369
La	12.4	11.7	12.8	10.4	12.7	12.6	9.5	9.3
Ce	27.1	26.4	28.4	24.9	28.3	24.5	22.7	21.7
Nd	12	12	15	15	15	13	14	16
Sm	2.93	2.90	3.17	2.97	2.97	2.73	2.94	2.86
Eu	0.98	0.99	1.01	1.01	0.99	0.90	0.99	1.00
Tb	0.43	0.37	0.47	0.45	0.42	0.38	0.41	0.44
Dy	3.1	2.7	3.1	2.9	2.9	2.6	2.7	2.8
Yb	1.83	1.81	1.96	1.77	1.69	1.68	1.72	1.73
Lu	0.25	0.09	0.16	0.25	0.15	0.14	0.16	0.15
Hf	3.5	3.4	3.8	3.1	3.5	3.3	2.9	2.7
Th	2.01	1.92	2.09	1.52	1.84	1.98	1.27	1.10
U	0.78	0.81	0.75	0.56	0.74	0.80	0.54	0.53
Eu/Eu*[b]	1.01	1.06	0.95	1.01	1.01	1.00	1.02	1.04
ΣREE's	61.0	59.0	66.1	59.7	65.1	58.5	55.1	56.0
Th/U	2.58	2.37	2.79	2.71	2.49	2.48	2.35	2.08

[a] In ppm, except Na, Ti, and Fe

All neutron activation analyses by F. Asaro and H. Bowman, Lawrence Berkeley Laboratory (Perlman and Asaro, 1969)

[b] Eu* is interpolated between Sm and Tb

Average counting uncertainties of one standard deviation are equal to the following percentages of the amounts present: Na (1%), Sc (1%), Ti (5%), V (15%), Cr (3%), Mn (1%), Fe (2%), Ni (10%), Zn (10%), Cs (10%), Ba (5%), La (20%), Ce (10%), Nd (15%), Sm (2%), Eu (2%), Tb (15%), Dy (20%), Yb (5%), Lu (15%), Hf (10%), Th (10%), U (5%)

Table 3. XRF analyses of whole rock samples

Col	9	6	17	15	18
Cu	27	35	30	23	18
Ga	19	19	17	17	18
Rb	19	20	21	16	21
Sr	568	593	531	584	609
Y	17	17	18	20	17
Zr	152	154	159	131	134
K/Rb	595	559	563	615	557
Rb/Sr	0.034	0.033	0.039	0.027	0.034
Col	2	7	11	13	
Cu	21	19	35	30	
Ga	19	20	18	21	
Rb	22	20	13	15	
Sr	625	602	568	571	
Y	15	17	20	16	
Zr	152	139	118	115	
K/Rb	550	598	677	603	
Rb/Sr	0.035	0.033	0.023	0.026	

Counting uncertainties of one standard deviation are: Sr (5%), Rb (13%), Y (22%), Zr (7%), Cu (15%), and Ga (10%) of the amounts present

Table 5. Neutron activation analyses of groundmass samples[a]

Col	9G	6G	17G	15G	2G	7G	11G
Na%	3.94	4.07	4.16	3.94	4.16	3.90	3.90
Sc	9.3	9.0	9.0	11.3	6.9	9.5	16.1
Ti%	0.40	0.35	0.34	0.38	0.25	0.33	0.54
V	110	93	62	118	55	99	301
Cr	8	4	4	6	3	4	29
Mn	645	570	535	732	670	613	810
Fe%	2.93	2.55	2.59	3.63	2.63	2.97	4.86
Ni	11	<10	10	16	12	<10	27
Zn	65	64	58	65	68	62	72
Cs	1.8	1.6	1.5	1.0	1.3	1.3	1.1
Ba	690	765	810	595	728	705	624
La	20.0	20.0	19.6	16.0	16.6	15.7	15.7
Ce	43.2	43.0	45.7	35.3	38.3	35.7	38.2
Nd	22	22	23	19	20	19	23
Sm	4.33	4.53	4.62	3.84	3.66	3.67	4.40
Eu	1.07	1.13	1.16	1.22	1.04	1.00	1.38
Tb	0.59	0.60	0.64	0.48	0.46	0.53	0.62
Dy	4.4	4.3	4.5	3.7	3.3	3.3	4.2
Yb	2.71	2.91	2.94	2.25	2.13	2.24	2.45
Lu	0.35	0.41	0.40	0.32	0.30	0.32	0.36
Hf	6.2	6.4	6.7	4.4	5.0	4.9	4.7
Th	3.62	3.84	3.86	2.38	2.92	3.17	2.40
U	1.27	1.38	1.42	0.91	1.09	1.15	0.88

[a] In ppm, except Na, Ti and Fe; uncertainties as in Table 2

Table 4. Wet chemical analyses of groundmass

Col	9G	6G	17G	15G	2G	7G	11G
SiO_2	67.65	68.70	68.82	61.90	66.80	66.70	60.45
TiO_2	0.70	0.73	0.70	0.76	0.61	0.61	1.11
Al_2O_3	15.37	15.10	15.10	16.99	16.31	16.08	16.91
Fe_2O_3	1.37	1.26	1.25	2.17	1.06	1.66	1.80
FeO	2.64	2.29	2.23	2.72	2.39	2.34	4.55
MnO	0.06	0.07	0.05	0.08	0.08	0.07	0.11
MgO	1.13	0.85	0.75	2.80	1.20	1.21	2.26
CaO	2.99	2.77	2.77	4.68	3.58	3.59	5.28
Na_2O	5.18	5.41	5.42	5.15	5.39	5.24	5.30
K_2O	2.53	2.51	2.51	1.77	2.19	2.18	1.74
P_2O_5	0.22	0.21	0.22	0.28	0.26	0.22	0.22
H_2O^+	–	–	–	0.71	–	–	–
H_2O^-	–	–	–	–	–	–	–
Total	99.84	99.90	99.82	100.01	99.87	99.90	99.73
CIPW norms (mol%)							
qz	18.18	19.14	19.41	10.67	16.24	17.20	7.53
or	14.95	14.81	14.83	10.44	12.88	12.86	10.26
ab	46.53	48.53	48.66	46.17	48.19	46.97	47.50
an	11.22	9.50	9.46	17.99	13.78	13.89	17.18
di	1.75	2.29	2.28	2.70	1.77	1.96	6.03
hy	4.50	2.96	2.62	8.14	4.64	4.08	7.63
mt	1.43	1.32	1.31	2.27	1.10	1.73	1.88
il	0.98	1.02	0.98	1.06	0.85	0.85	1.54
ap	0.46	0.44	0.46	0.58	0.54	0.46	0.46

all trend toward more silicic compositions. Such compositional trends are generally disrupted by caldera forming eruptive events, which usually involve silicic magmas. The common occurrence of summit calderas at andesitic composite volcanoes argues strongly for the presence of relatively large, near surface magma chambers below or within the volcanic pile. Trends toward more evolved eruptive compositions with time imply that some mechanism such as crystal fractionation is operating within these chambers. Wide compositional alternations in erupted magma types, however, demonstrate that the volcanoes periodically receive pulses of relatively basic magma from depth. Realistic chemical models for temporal variations in eruptive composition at andesitic volcanoes, therefore, must be capable of simultaneously treating crystal fractionation, magma mixing, and other processes (O'Hara, 1977).

Selected major and trace element concentrations for the post-caldera andesites of Volcán Colima are plotted versus eruption date in Figs. 5 and 6. Arbitrary, prehistoric eruption dates are used for Col 7, 11, and 13. Temporal variations in the investigated suite can be viewed on three time scales, covering: (1) all of post-caldera time, (2) a single eruptive cycle, and (3) a single eruption.

The olivine andesites (Col 11 and 13) are both the oldest and the most basic of the investigated samples. In a general way, then, compositions have become more evolved through the life of the post-caldera cone, but reversals in this trend have also occurred (i.e., Col 15).

Correlation between temporal variations in magma composition and the historical eruptive cycles of Volcán Colima is made difficult by a lack of adequate sample control. No samples can be positively correlated with known eruptions prior to 1869, and the numerous pyroclastic eruptions between 1869 and 1913 (Fig. 3)

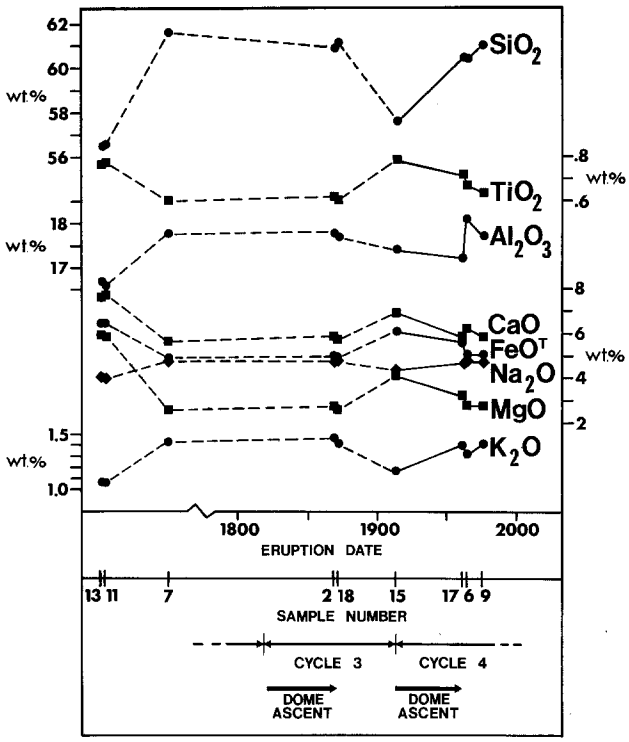

Fig. 5. Selected major element analyses of whole rock samples plotted versus *eruption date. Dashed lines* indicate inadequate sample control between points

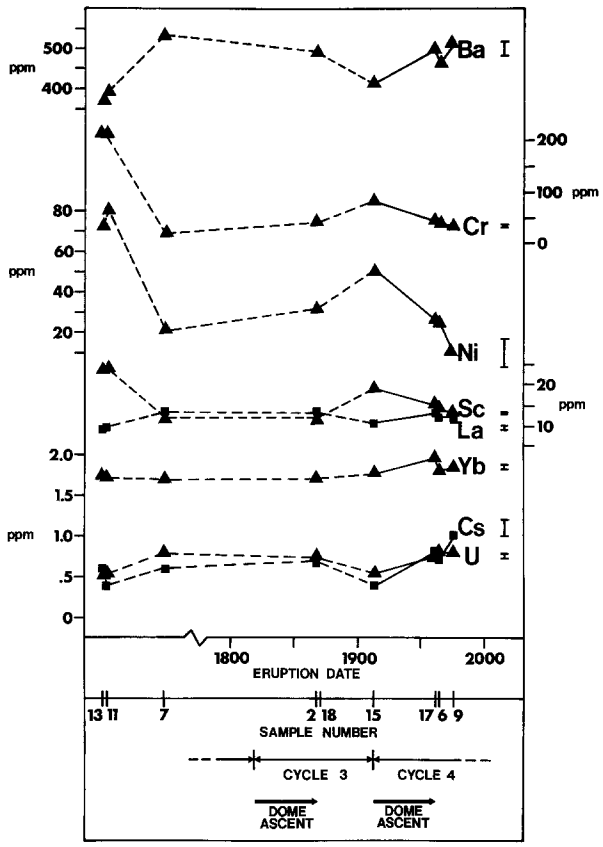

Fig. 6. Selected trace element analyses of whole rock samples plotted versus *eruption date. Dashed lines* indicate inadequate sample control between points. Error bars reflect uncertainties listed in Table 2

are not represented in the sample suite. A reliable, nearly complete record is only available from 1913 to the present. Over that time, from the final ashflow eruption of the third eruptive cycle (Col 15) through the fourth cycle andesites (Col 17, 6, and 9), there have been fairly continuous increases in SiO_2, Ba, and Cs, and decreases in TiO_2, FeO^T, MgO, Ni, Cr, and Sc. Deviations from this overall trend may reflect local crystal accumulation or separation as suggested by the relatively high Na, Ca, Al, and Sr, and low Ti, Fe, and Mg contents of Col 6. Major and trace element crystal fractionation models for the generation of compositional trends from Col 15 to Col 9 are presented in a later section. Because of the limited data base available, no firm conclusions can be drawn concerning possible controls on eruptive periodicity imposed by magma compositions. The major ashflow eruption of 1913, which terminated the third historical eruptive cycle, involved one of the most basic of the post-caldera andesites. It may be speculated that through the active phase of an eruptive cycle, magma compositions become progressively more evolved with time (Col 17 to Col 9), but that the cycle ending ashflow activity (Col 15) abruptly reverses this trend, halting activity for 50 or more years. Analysis of future eruptive products from Volcán Colima, particularly of the anticipated ashflow eruption to end the present eruptive cycle, will allow this hypothesis to be tested.

Compositional variations with time during a single eruption can be radically different from variations observed through a sequence of eruptions over a period of hundreds to thousands of years (Katsui et al., 1975). Two of Colima's major lava eruptions have been sampled and analyzed in duplicate. Col 11 and 13 are from different lobes of the olivine-andesites which filled the northwestern portion of the caldera, and Col 18 and 2 are from the two different hornblende-andesite flow lobes erupted in 1869. Despite rather large differences in compositions and zoning patterns of mineral phases in the sample pairs, whole rock major and trace element compositions are nearly identical (Tables 1–3). In two tested cases, then, there appears to be little variation in chemical composition through the course of lava eruptions at Volcán Colima. Fairbrothers et al. (1978) noted a similar degree of homogeneity within the 0.01 km^3 andesitic flow erupted from Boqueron Volcano, El Salvador, in 1917. Nelson (1979) analyzed four samples from the 1.1 km^3 dacitic lava erupted from Volcán Ceboruco, Mexico, in 1870. He noted a slight decrease in SiO_2 through the eruption (0.6 wt.%), but no systematic variations of other major or trace elements.

Mineralogy and Petrology

The nine samples considered in this study are readily divisible into hornblende-andesites (Col 9, 6, 17, 15, 18, 2, and 7) and olivine-andesites (Col 11 and 13) based on the mutually exclusive presence of either mineral as a stable, crystallizing phase. In addition, each sample contains phenocrysts and microphenocrysts of plagioclase, orthopyroxene, clinopyroxene, and titanomagnetite, and very

Table 6. Modal analyses (vol.%) (> 700 points counted)

Col	Eruption date	plag	cpx	opx	oxides	hbd	oliv	grndm	sum xlls
9_{ph}	1975	30.4	1.8	1.9	–	0.8	tr	52.8	47.2
9_{mp}		7.7	1.2	1.2	2.1	0.1	–		
6_{ph}	1962	30.0	3.2	2.7	0.1	0.6	tr	49.5	50.5
6_{mp}		8.1	0.8	2.6	2.4	–	–		
17_{ph}	1961	31.8	2.0	3.8	0.1	1.0	tr	48.4	51.6
17_{mp}		8.4	0.7	2.3	1.5	–	–		
15_{ph}	1913	14.7	0.4	2.6	–	3.6	tr	70.4	29.6
15_{mp}		3.6	1.8	1.8	0.8	0.4	–		
18_{ph}	1869?	13.9	0.5	0.6	0.4	4.9	tr	64.2	35.8
18_{mp}		13.8	0.1	1.1	0.4	0.1	–		
2_{ph}	1869	23.1	1.6	0.9	0.2	3.5	tr	62.0	38.0
2_{mp}		4.8	0.6	1.5	1.7	0.1	–		
7_{ph}	?	22.2	1.8	2.9	–	1.5	tr	61.3	38.7
7_{mp}		5.8	1.3	1.2	1.8	0.2	–		
11_{ph}	?	21.9	4.5	3.2	–	–	1.3	60.0	40.0
11_{mp}		2.9	2.5	2.1	–	–	1.6		
13_{ph}	?	23.7	2.0	2.5	–	–	2.0	54.9	45.1
13_{mp}		7.8	3.9	2.0	0.7	–	0.5		

ph: phenocrysts (> 0.3 mm); mp: microphenocrysts (> 0.03 mm)

rare microphenocrysts of hematite-ilmenite set in a microcrystalline to glassy groundmass. All samples have glomeroporphyritic textures. Following the grain size conventions of Wilcox (1954), phenocrysts are defined as greater than 0.3 mm in maximum dimension and microphenocrysts as greater than 0.03 mm.

Point counted modal analyses for each sample are listed in Table 6 in order of increasing sample age. With the exception of hornblende, all phases present as phenocrysts and microphenocrysts are present in the groundmass (less than 0.03 mm). Both crystals and glass are included in the groundmass component of Table 6. Owing to the microscoriaceous nature of Col 15, its groundmass percentage is less certain. Significant features of the data include (1) the mutually exclusive occurrence of stable hornblende and olivine, (2) the consistently high crystal contents (greater than 0.03 mm diam.) in the suite, ranging up to 52 vol.%, and (3) the reduced hornblende contents (0.6–1.0 vol.%) and higher total crystal contents (47.2–51.6 vol.%) in the fourth cycle hornblende-andesites, Col 9, 6, and 17, versus earlier hornblende-andesites of similar bulk composition, Col 18, 2, and 7 (1.7–5.0 vol.% hbd; 35.8–38.7 vol.% crystals).

Plagioclase

Plagioclase is the most abundant crystalline phase in each sample. The largest grains are generally greater than 3 mm in length, although close inspection often reveals these to be annealed composites of several smaller grains. Rounded to irregular brown glass inclusions are often present within the plagioclase and can be highly concentrated in crystal cores or in one or more distinct zones paralleling crystal margins. It is common to find plagioclase crystals with widely varying glass inclusion densities and styles within a single thin section. A crude estimate of the volume percentage of glass inclusions within plagioclase is listed for each sample in Table 7. Brown glass inclusions are most abundant in the oldest, most basic, olivine-andesites, where heavily riddled cores are surrounded by clear, less calcic, oscillatory zoned rims. Glass inclusions are least abundant in the plagioclase of the most silicic samples, including the 1975–1976 andesite, Col 9. Following glass, apatite is the next most abundant included phase. On average, apatite accounts for less than 0.05 vol.% of the plagioclase. It occurs as needles up to 0.1 mm in length, which are occassionally concentrated in crystal cores, but more commonly in distinct zones paralleling crystal margins. In the latter occurrence, the needles are usually oriented tangentially to the plagioclase rims. Any other coexisting crystalline phase may be included in the plagioclase phenocryst rims, but these are rare.

As is characteristic of calc-alkaline andesites, the plagioclase in these samples displays complex oscillatory zoning, which is usually most pronounced on crystal margins, where more than 40 distinct zones may be present. Commonly a clear, oscillatory zoned margin with a trend of decreasing calcium toward the rim surrounds a more calcic core which is either (1) inclusion free, (2) separated from the clear margin by a penultimate zone of glass inclusions, or (3) heavily riddled with brown glass inclusions.

Table 7 lists average microprobe analyses of plagioclase phenocryst rims and the most sodic and most calcic point analyses in each sample. Analyses are listed in order of increasing sample age. All samples contain normally zoned plagioclase on average. Microphenocryst analyses (unreported) of plagioclase and all other phases overlap with those of phenocryst rims in each sample. Neutron activation analyses of hand picked plagioclase separates from seven of the samples are given in Table 8.

Orthopyroxene

Orthopyroxene is usually the most abundant mafic mineral in Colima's post-caldera andesites. It is generally less than 2 mm in

Table 7. Microprobe analyses of plagioclase

Col	9r	9ab	9an	6r	6ab	6an	17r	17ab	17an	15r	15ab	15an	18r	18ab	18an
SiO_2	55.95	57.02	51.57	55.25	56.72	53.43	54.58	59.36	45.86	54.65	57.27	51.83	54.02	57.93	51.50
Al_2O_3	28.14	26.86	31.26	27.87	27.42	29.56	28.68	25.03	34.49	28.64	27.08	30.15	29.18	26.99	30.44
Fe_2O_3	0.53	0.53	0.54	0.57	0.53	0.59	0.55	0.59	0.41	0.55	0.51	0.52	0.57	0.47	0.51
BaO	0.03	0.05	0.00	0.03	0.06	0.00	0.04	0.12	0.01	0.03	0.06	0.00	0.03	0.05	0.01
SrO	0.09	0.02	0.04	0.08	0.03	0.07	0.11	0.05	0.11	0.09	0.13	0.07	0.10	0.00	0.13
CaO	10.11	8.82	13.02	9.90	9.42	12.14	10.51	6.53	16.87	10.92	9.52	13.90	11.64	8.90	13.03
Na_2O	5.82	6.62	4.31	6.13	6.29	4.87	5.65	7.95	2.20	5.28	6.00	3.75	5.18	6.62	4.43
K_2O	0.22	0.25	0.12	0.23	0.31	0.15	0.21	0.50	0.04	0.18	0.22	0.07	0.16	0.27	0.12
Total	100.89	100.17	100.86	100.06	100.78	100.81	100.33	100.13	99.99	100.34	100.79	100.29	100.88	101.23	100.17
X_{an}	0.484	0.418	0.621	0.466	0.445	0.575	0.501	0.304	0.807	0.528	0.461	0.669	0.549	0.420	0.615
X_{ab}	0.504	0.568	0.372	0.522	0.538	0.417	0.487	0.669	0.191	0.462	0.526	0.327	0.442	0.565	0.378
X_{or}	0.013	0.014	0.007	0.013	0.017	0.009	0.012	0.028	0.022	0.010	0.013	0.004	0.009	0.015	0.007
GI%			5			10			10			25			10

Col.	2r	2ab	2an	7r	7ab	7an	11r	11ab	11an	13r	13ab	13an
SiO_2	54.57	55.66	45.39	54.28	56.33	51.94	52.88	54.73	49.11	53.58	56.57	47.52
Al_2O_3	29.47	28.02	35.43	29.14	27.07	30.85	29.64	28.38	32.34	29.52	27.43	33.86
Fe_2O_3	0.56	0.68	0.48	0.57	0.53	0.52	0.73	0.83	0.57	0.72	0.78	0.43
BaO	0.03	0.04	0.02	0.04	0.11	0.06	0.02	0.01	0.01	0.02	0.10	0.00
SrO	0.10	0.07	0.06	0.11	0.08	0.13	0.08	0.08	0.06	0.08	0.06	0.10
CaO	11.36	9.78	17.80	11.01	9.02	12.62	12.12	10.36	15.14	12.11	9.43	16.75
Na_2O	5.26	6.02	1.75	5.50	6.74	4.50	4.93	5.68	3.30	4.89	5.65	2.41
K_2O	0.20	0.28	0.03	0.25	0.25	0.21	0.18	0.24	0.09	0.18	0.74	0.04
Total	101.55	100.55	100.96	100.90	100.13	100.83	100.58	100.31	100.62	101.10	100.76	101.11
X_{an}	0.538	0.466	0.848	0.518	0.419	0.601	0.570	0.495	0.714	0.572	0.459	0.792
X_{ab}	0.451	0.519	0.151	0.468	0.567	0.388	0.420	0.491	0.281	0.418	0.498	0.206
X_{or}	0.011	0.016	0.002	0.014	0.014	0.012	0.010	0.014	0.005	0.010	0.043	0.002
GI%			15			5			45			45

r: average of phenocryst rims; ab: most sodic point analysis; an: most calcic point analysis
GI%: Estimate of glass inclusion density in plagioclase

maximum dimension and invariably displays pink-green pleochroism. Titanomagnetite is a common included phase in the rims of both orthopyroxene and clinopyroxene, occurring as grains up to 0.2 mm in diameter. Tiny (0.1 mm long) apatite needles and glass are less common as inclusions, although individual crystals can be literally riddled with apatite. Similar to their occurrence within plagioclase, apatite needles and glass inclusions in pyroxenes are often concentrated in crystal cores or in thin zones paralleling crystal margins.

Table 9 lists average microprobe analyses of orthopyroxene phenocryst rims and cores in order of increasing sample age. Total compositional variation of orthopyroxene in a given sample is never more than 10 mol% $MgSiO_3$. Differences between average rim and core compositions are less than 2 mol% (Mg) for the hornblende-andesites and less than 6 mol% (Mg) for the olivine-andesites. Only those samples belonging to the fourth eruptive cycle (Col 9, 6, and 17) dominantly contain normally zoned orthopyroxenes, with relatively iron rich rims. Almost all orthopyroxenes in pre-1961 samples have relatively magnesium rich rims. Magnesium enriched rims are most pronounced in the oldest of the samples, the olivine-andesites Col 11 and 13. In addition, approximately 5% of the orthopyroxenes in these samples are jacketed by thin clinopyroxene rims instead of by the Mg-rich orthopyroxene rims. This phenomenon of clinopyroxene jacketing is not observed in the hornblende-andesites. Neutron activation analyses of hand picked orthopyroxene separates from six of the samples are listed in Table 10. The somewhat high Na contents for Col 6 and 17 orthopyroxene in Table 10 apparently reflect minor groundmass contamination.

Clinopyroxene (Augite)

Augite is generally subordinate in amount to orthopyroxene, but usually predominates within crystal clusters as noted by Nelson (1979) at Volcán Ceboruco. Augite is less than 2 mm in size as phenocrysts, though slightly larger within clusters. Inclusion patterns are similar to those described for orthopyroxenes.

Table 8. Neutron activation analyses of plagioclase[a]

Col	9	6	17	15	2	7	11
Na%	4.04	4.00	4.00	3.78	3.92	4.08	3.53
Sc	0.24	0.16	0.13	0.13	0.17	0.16	0.28
Ti%	< 0.03	< 0.03	< 0.04	< 0.06	< 0.05	< 0.05	< 0.04
V	< 25	< 30	< 25	< 18	< 25	46	< 22
Cr	0.5	< 1	< 0.3	0.4	0.2	0.4	0.7
Mn	45	39	38	40	45	41	38
Fe%	0.39	0.38	0.39	0.36	0.41	0.40	0.47
Ni	< 2	2.4	< 2	< 1	2.6	6.1	3.0
Zn	10	16	10	11	17	10	9
Cs	< 0.2	< 0.3	< 0.3	< 0.3	< 0.4	< 0.3	0.04
Ba	250	60	120	211	58	73	52
La	2.7	4.1	3.2	2.3	2.9	3.2	2.0
Ce	5.5	6.0	5.5	4.7	5.7	6.3	4.6
Nd	2.7	3.6	1.9	1.6	3.2	2.8	3.0
Sm	0.34	0.46	0.33	0.27	0.32	0.38	0.31
Eu	0.72	0.71	0.85	0.71	0.64	0.70	0.49
Tb	0.04	0.03	0,03	0.03	0.03	0.04	0.03
Dy	0.2	0.2	0.3	< 0.12	0.3	0.2	0.2
Yb	0.06	0.03	0.03	0.04	0.05	0.03	0.03
Lu	0.03	< 0.03	< 0.02	< 0.02	< 0.03	< 0.03	< 0.02
Hf	0.15	0.06	0.06	0.03	0.11	0.08	0.07
Th	0.02	< 0.05	0.04	0.01	< 0.02	< 0.02	< 0.02

[a] In ppm, except Na, Ti, and Fe; uncertainties as listed in Table 2

Table 10. Neutron activation analyses of orthopyroxene[a]

Col	9	6	17	2	7	11
Na%	0.21	0.83	0.48	0.19	0.12	0.13
Sc	37.9	34.7	36.2	32.6	35.4	35.8
Ti%	0.13	0.19	0.14	0.12	0.15	0.12
V	132	136	115	119	108	140
Cr	234	84	181	429	443	721
Mn	4,124	3,747	3,824	3,438	3,601	2,768
Fe%	12.9	11.2	11.9	12.0	12.4	11.2
Ni	140	79	131	254	237	400
Zn	266	248	257	239	244	188
Cs	< 0.6	< 0.5	< 0.6	< 0.4	< 0.4	0.5
Ba	23	172	98	38	31	28
La	1.9	5.9	3.9	1.7	0.9	< 0.5
Ce	5.7	14.2	8.4	2.4	2.4	< 0.8
Nd	3.5	9.5	5.4	2.2	2.4	1.2
Sm	0.95	1.96	1.27	0.41	0.42	0.27
Eu	0.22	0.47	0.30	0.11	0.11	0.09
Tb	0.20	0.29	0.26	0.13	0.13	0.09
Dy	1.8	2.4	1.6	1.2	1.0	0.9
Yb	1.14	1.64	1.33	0.81	0.93	0.72
Lu	0.20	0.28	0.23	0.15	0.16	0.11
Hf	0.3	1.4	0.7	0.2	< 0.1	0.2
Th	0.21	0.84	0.30	0.12	0.16	0.13

[a] In ppm, except for Na, Ti, and Fe; uncertainties as in Table 2

Table 9. Average microprobe analyses of orthopyroxene

Col	9r	9c	6r	6c	17r	17c	15r	15c	18r	18c	2r	2c	7r	7c	11r	11c	13r	13c
SiO_2	53.17	53.24	52.70	52.82	53.10	52.98	52.75	52.81	53.30	52.93	53.27	52.69	53.28	53.31	53.87	53.64	54.01	53.78
TiO_2	0.26	0.28	0.30	0.26	0.29	0.25	0.26	0.24	0.22	0.22	0.23	0.28	0.25	0.27	0.29	0.24	0.28	0.23
Al_2O_3	1.27	1.50	1.26	1.17	1.15	1.25	1.51	1.05	0.65	1.20	1.27	1.40	1.02	1.09	1.91	1.30	1.75	1.15
FeO	17.90	17.17	17.74	17.40	17.36	16.38	16.00	16.35	16.61	16.90	17.09	17.66	17.19	17.36	14.29	16.32	13.67	17.11
MnO	0.52	0.49	0.60	0.55	0.47	0.40	0.43	0.44	0.46	0.53	0.50	0.52	0.50	0.50	0.28	0.41	0.29	0.49
MgO	25.30	25.87	26.02	26.47	26.21	27.12	27.51	27.40	26.94	26.79	26.57	26.03	26.24	26.19	27.99	26.94	28.98	26.37
CaO	1.25	1.34	1.35	1.35	1.33	1.25	1.23	1.24	1.33	1.31	1.23	1.21	1.32	1.30	1.38	1.32	1.51	1.34
Na_2O	0.00	0.00	0.00	0.00	0.01	0.00	0.00	0.00	0.00	0.00	0.00	0.00	0.00	0.00	0.01	0.00	0.00	0.00
Total	99.67	99.89	99.97	100.02	99.92	99.63	99.69	99.53	99.51	99.88	100.16	99.79	99.80	100.02	100.02	100.17	100.49	100.47
X_{en}	0.698	0.709	0.704	0.712	0.710	0.729	0.736	0.731	0.724	0.720	0.717	0.707	0.712	0.710	0.757	0.727	0.768	0.714
X_{fs}	0.277	0.264	0.269	0.262	0.264	0.247	0.240	0.245	0.251	0.255	0.259	0.269	0.262	0.264	0.217	0.247	0.203	0.260
X_{wo}	0.025	0.026	0.026	0.026	0.026	0.024	0.024	0.024	0.026	0.025	0.024	0.024	0.026	0.025	0.027	0.026	0.029	0.026
high X_{en}		0.743		0.726		0.768		0.752		0.795		0.748		0.727		0.781		0.786
low X_{en}		0.680		0.696		0.693		0.704		0.699		0.670		0.688		0.677		0.702
a_{en}	0.671	0.679	0.676	0.685	0.684	0.702	0.705	0.707	0.706	0.693	0.690	0.678	0.689	0.685	0.720	0.700	0.733	0.689
a_{fs}	0.266	0.253	0.258	0.252	0.254	0.238	0.230	0.237	0.244	0.245	0.249	0.258	0.253	0.255	0.206	0.238	0.194	0.251

r: average of phenocryst rims; c: average of phenocryst cores; a_{en} and a_{fs} calculated after Carmichael et al. (1977)

Table 11. Average microprobe analyses of clinopyroxene

Col	9r	9c	6	17r	17c	15r	15c	18	2	7	11r	11c	13r	13c
SiO_2	51.82	51.75	51.07	51.50	52.50	51.05	50.63	50.95	50.97	51.70	51.22	50.47	52.13	51.95
TiO_2	0.46	0.59	0.56	0.67	0.44	0.58	0.69	0.56	0.55	0.49	0.66	0.70	0.60	0.49
Al_2O_3	2.54	2.67	2.21	2.78	1.79	3.61	3.71	2.37	2.86	2.19	3.61	3.91	2.36	3.43
FeO	9.04	8.63	8.91	8.84	7.56	7.34	7.91	9.04	8.68	8.60	7.81	8.77	8.22	6.24
MnO	0.03	0.29	0.30	0.28	0.22	0.24	0.21	0.29	0.25	0.27	0.16	0.21	0.23	0.17
MgO	14.75	15.18	15.48	15.21	16.29	16.02	15.68	15.30	15.31	15.43	15.76	14.77	16.58	17.06
NiO	0.01	0.01	0.02	0.01	0.00	0.02	0.02	0.00	0.01	0.01	0.03	0.04	0.00	0.02
CaO	20.21	20.23	20.14	20.08	20.66	20.13	20.29	20.43	20.56	20.43	20.22	20.18	19.82	20.46
Na_2O	0.47	0.45	0.44	0.50	0.42	0.41	0.44	0.42	0.48	0.46	0.48	0.51	0.35	0.37
Total	99.33	99.80	99.13	99.87	99.88	99.40	99.58	99.36	99.67	99.58	99.95	99.56	100.29	100.19
X_{en}	0.429	0.439	0.443	0.440	0.460	0.463	0.452	0.436	0.438	0.442	0.455	0.432	0.468	0.484
X_{fs}	0.148	0.140	0.143	0.143	0.120	0.119	0.128	0.145	0.139	0.138	0.126	0.144	0.130	0.099
X_{wo}	0.423	0.421	0.414	0.417	0.420	0.418	0.420	0.419	0.423	0.420	0.419	0.424	0.402	0.417
high X_{en}		0.478	0.452		0.495		0.485	0.449	0.441	0.459		0.473		0.507
low X_{en}		0.424	0.439		0.443		0.451	0.443	0.419	0.441		0.437		0.474

r: average of phenocryst rims; c: average of phenocryst cores

Table 12. Neutron activation analyses of clinopyroxene[a]

Col	9	6	17	2	7	11
Na%	0.42	0.42	0.46	0.42	0.39	0.39
Sc	109.0	112.3	112.5	112.5	116.8	110.7
Ti%	0.29	0.31	0.21	0.28	0.32	0.27
V	275	299	275	288	273	339
Cr	640	584	650	734	504	1,245
Mn	2,176	2,207	2,210	2,228	2,320	1,873
Fe%	6.3	6.4	6.3	6.7	6.4	5.9
Ni	60	46	90	72	63	153
Zn	690	569	718	439	656	686
Cs	<0.3	<0.5	<0.3	<0.4	<0.4	0.7
Ba	25	37	20	<20	11	24
La	3.7	2.8	2.7	3.8	2.5	2.2
Ce	10.0	10.4	10.8	12.7	12.8	7.8
Nd	10	14	12	14	13	10
Sm	4.25	4.35	4.28	4.57	4.61	3.44
Eu	1.16	1.21	1.19	1.27	1.19	0.99
Tb	0.77	0.89	0.77	0.90	0.88	0.69
Dy	6.0	6.1	6.1	6.0	6.3	5.2
Yb	2.80	2.81	2.74	2.80	2.97	2.36
Lu	0.39	0.39	0.38	0.39	0.44	0.31
Hf	1.4	1.5	1.4	1.7	1.4	1.2
Th	–	<0.5	–	<0.2	<0.5	<0.1

[a] In ppm, except for Na, Ti, and Fe; uncertainties as in Table 2

Average microprobe analyses of augite phenocryst rims and cores are listed in Table 11 in order of increasing sample age. Compositional zoning is less pronounced in Colima's augites than in the orthopyroxenes, and if no significant rim to core zoning was detected in a particular sample, a single composition is given in Table 11. Total variation in each sample is always less than 5 mol% $MgSiO_3$. Average rims and cores always differ by less than 2 mol% (Mg). Augite phenocrysts are normally zoned to unzoned in the samples belonging to the fourth eruptive cycle (Col 9, 6, and 17). Older samples have normally zoned, unzoned and reversely zoned augites. Of paricular interest are the zoning patterns in the olivine-andesites. Nearly all of the augite in Col 11, like the orthopyroxene, is reversely zoned with well developed, Mg-rich rims. Augite in Col 13, however, is largely normally zoned. Such dissimilar phenocryst zoning patterns are surprising in samples of nearly identical bulk composition (Tables 1–3). Neutron activation analyses of hand picked augite separates from six of the samples are listed in Table 12.

Hornblende

Basaltic hornblende with strong, reddish-brown pleochroism occurs as large crystals up to 4 mm i.d. In all but the quickly quenched scoria sample, Col 15, the hornblende is surrounded by either a reaction rim of opacite (fine-grained magnetite) up to 0.15 mm thick, or a granular reaction corona of pyroxene, plagioclase, and magnetite. Both styles of reaction occur within a single thin section, although reaction to opacite is restricted to microphenocrysts and the rims of phenocrysts, suggesting that it is the initial stage of hornblende decomposition. In many instances, hornblende crystals have totally reacted to a granular, multiphase pseudomorph. These aggregates are easily recognized as hornblende pseudomorphs on the basis of their fine-grained, granular texture and external morphology. They are quite unlike the coarse grained, often clinopyroxene-dominated crystal clusters which are also present in all post-caldera andesites at Volcán Colima. Stewart (1975) suggested such coarse grained crystal clusters in andesites as possible hornblende decomposition products. Textural patterns in Colima's hornblende-andesites do not support this interpretation. Garcia and Jacobson (1979) also reject hornblende decomposition as the origin of crystal clots in a suite of Cascade andesites. Hornblende microphenocrysts rarely survive eruptive reaction in Colima's lavas. The absence of hornblende reaction relationships in the quickly quenched scoria of Col 15 supports the concept that this style of hydroxy-hornblende decomposition occurs during eruption and cooling under low pressure conditions (Kuno, 1950). Inclusions of titanomagnetite, pyroxene, and plagioclase are occasionally present in Colima's hornblendes, but generally the hornblende occurs as large, inclusion-free crystals.

Table 13. Average microprobe analyses of hornblende

Col	6	17	15	18	2	7
SiO_2	42.41	42.50	42.61	43.99	43.15	42.65
TiO_2	2.48	2.67	2.68	2.36	2.97	2.33
Al_2O_3	12.08	12.82	11.75	10.92	11.47	11.83
FeO	12.78	10.60	12.26	11.89	11.83	12.04
MnO	0.18	0.15	0.18	0.25	0.24	0.17
MgO	13.79	14.94	13.98	14.65	14.23	14.54
NiO	0.02	0.03	0.03	0.01	0.00	0.01
CaO	11.11	11.28	11.14	11.25	11.35	11.32
Na_2O	2.66	2.82	2.56	2.50	2.67	2.65
K_2O	0.38	0.40	0.41	0.37	0.45	0.40
F	0.12	0.13	0.08	0.10	0.11	0.12
Cl	0.05	0.02	0.03	0.03	0.04	0.03
H_2O[a]	2.00	2.00	2.00	2.00	2.00	2.00
Total	100.06	100.36	99.71	100.32	100.51	100.09
high MgO	14.24	15.50	14.63	14.85	14.55	15.29
low MgO	12.97	14.27	13.55	14.55	13.81	14.19
$X^{hbd}_{cumm} \times 10^5$	6.2	7.1	8.3	14.9	7.7	8.7

[a] All H_2O assumed equal to 2.00 wt.%
$X^{hbd}_{cumm} = (X^{A}_{vac})(X^{M}_{Mg})^7(X^{T}_{Si})^8(X^{V}_{OH})^2$

Table 14. Neutron activation analyses of hornblende and olivine[a]

Col	6 h	17 h	15 h	2 h	7 h	11 ol
Na%	1.96	2.02	2.02	2.03	2.01	0.05
Sc	92.6	93.0	91.6	93.3	90.6	4.8
Ti%	1.52	1.56	1.64	1.70	1.50	<0.02
V	655	706	738	709	639	25
Cr	205	244	186	206	359	974
Mn	1,317	1,266	1,353	1,369	1,317	1,716
Fe%	9.0	8.9	9.2	9.4	9.0	11.2
Ni	139	157	115	146	138	1,563
Zn	318	412	526	537	542	107
Cs	<0.4	<0.3	0.5	<0.2	<0.3	<0.3
Ba	128	118	133	111	113	<10
La	2.7	2.9	3.0	3.1	3.0	<0.3
Ce	14.0	13.2	13.2	13.0	12.2	<0.5
Nd	17.4	16.2	17.1	19	16.7	<0.5
Sm	5.95	5.34	6.03	6.34	5.54	0.041
Eu	1.88	1.77	1.96	2.01	1.79	<0.04
Tb	1.16	0.96	0.95	1.13	1.01	<0.07
Dy	7.6	7.6	8.1	8.2	7.2	<0.4
Yb	3.44	3.14	3.42	3.43	3.21	0.08
Lu	0.44	0.40	0.47	0.49	0.45	<0.03
Hf	2.2	2.4	2.3	2.1	2.2	<0.07
Th	0.7	<0.5	0.59	0.45	0.45	<0.05

h: hornblende; ol: olivine

[a] In ppm, except for Na, Ti, and Fe; uncertainties as in Table 2

Table 15. Average microprobe analyses of olivine

Col	9x	17x	11r	11c	11x	13r	13c	13x
SiO_2	37.94	39.00	38.14	38.40	39.25	38.53	39.15	40.60
TiO_2	0.05	0.00	0.03	0.02	0.02	0.02	0.02	0.02
FeO	23.76	18.01	24.28	22.94	11.66	22.15	19.49	12.57
MnO	0.43	0.32	0.40	0.37	0.15	0.38	0.29	0.19
MgO	37.69	42.76	37.44	38.70	47.25	39.47	42.07	47.60
NiO	0.14	0.09	0.07	0.10	0.37	0.10	0.14	0.24
CaO	0.09	0.09	0.17	0.15	0.12	0.15	0.14	0.15
Total	100.10	100.27	100.52	100.68	98.83	100.80	101.30	101.37
X_{fo}	0.739	0.809	0.733	0.751	0.878	0.761	0.794	0.871
X_{fa}	0.261	0.191	0.267	0.250	0.122	0.240	0.206	0.129
high X_{fo}	0.742	0.808			0.877			0.869
low X_{fo}	0.737	0.793			0.697			0.717
a_{fo}	0.546	0.654	0.538	0.563	0.771	0.578	0.630	0.759
a_{fa}	0.068	0.037	0.071	0.062	0.015	0.057	0.042	0.017

a_{fo} and a_{fa} calculated after Carmichael et al. (1977)
r: average of phenocryst rims; c: average of phenocryst cores;
x: average of cores of reacting xenocrysts

No reliable analysis of phenocrystic hornblende was obtained for Col 9, the small percentage of hornblende in this sample having almost completely reacted on eruption. Consistent rim to core zoning was not detected in the analyzed hornblende of any sample. Average microprobe analyses of hornblendes and their ranges in MgO content are listed in Table 13 in order of increasing sample age. Neutron activation analyses of hand picked hornblende separates from five samples are listed in Table 14.

Olivine

In Col 11 and 13, olivine occurs as rounded to euhedral microphenocrysts and phenocrysts up to 3.5 mm long, and also as resorbed, reacted xenocrysts. Olivine is also present in all of the hornblende-andesites as rare, remnant xenocrysts rimmed by pyroxenes. Olivines contain only occasional titanomagnetite and glass inclusions.

Table 16. Average microprobe analyses of Fe–Ti oxides

Col	9m	9h	6m	17m	15m	18m	2m	7m	11m[a]	11m[b]	13m[a]	13m[b]
SiO_2	0.06	0.00	0.14	0.10	0.04	0.10	0.11	0.13	0.19	0.19	0.18	0.15
TiO_2	9.82	39.22	11.04	12.22	6.95	7.92	7.63	8.86	10.70	9.60	12.61	10.44
Al_2O_3	2.31	0.00	2.41	1.32	3.79	2.79	2.45	2.25	2.98	3.84	1.42	2.58
V_2O_3	0.58	0.20	0.51	0.50	0.60	0.52	0.56	0.54	0.78	0.62	0.75	0.64
Cr_2O_3	0.11	0.05	0.09	0.10	0.31	0.10	0.12	0.08	1.36	4.15	1.27	3.64
FeO	81.19	55.73	79.22	80.02	80.21	81.06	82.73	80.34	75.93	74.12	76.55	74.20
MnO	0.40	0.30	0.44	0.51	0.37	0.35	0.39	0.36	0.34	0.30	0.48	0.37
MgO	1.90	2.48	1.86	1.60	3.02	2.39	1.80	1.74	3.59	3.89	2.52	3.96
CaO	0.03	0.00	0.03	0.03	0.00	0.03	0.01	0.01	0.06	0.01	0.03	0.01
Total	95.82	97.98	95.23	95.90	94.71	94.75	95.24	93.76	95.15	96.09	95.04	95.36
Recalculated analyses												
Fe_2O_3	48.34	27.99	45.07	44.44	52.05	51.08	52.08	48.66	44.39	43.47	41.85	43.45
FeO	37.70	30.55	38.67	40.04	33.38	35.09	35.87	36.56	35.98	35.01	38.90	35.10
Total	101.24	100.78	100.26	100.85	100.51	100.38	101.02	99.19	100.38	101.08	100.00	100.34
high TiO_2	10.38	41.23	12.99	14.45	8.20	10.28	8.72	10.64	14.10	10.34	13.81	11.01
low TiO_2	9.45	36.74	9.92	10.88	5.61	6.51	7.02	7.76	7.72	8.50	10.89	9.21
a_{mt}	0.667		0.627	0.619	0.714	0.707	0.722	0.686	0.607	0.586	0.582	0.593

m: titanomagnetite; H: hematite-ilmenite

[a] Titanomagnetite in groundmass and included in pyroxenes
[b] Titanomagnetite included in olivine

Table 17. Neutron activation analysis of titanomagnetite[a]

Col	6	17	2	7	11
Na%	0.37	0.53	0.39	0.52	1.55
Sc	29	30	18	24	28
Ti%	5.0	4.6	3.5	1.8	2.7
V	3,600	3,350	2,920	3,400	2,630
Cr	660	604	1,020	530	2,700
Mn	3,700	3,770	–	–	3,320
Fe%	52.3	49.0	56.0	50.0	35.1
Ni	147	190	157	125	260
Zn	805	740	680	730	390
Cs	<1	<0.7	<0.5	<0.5	<0.5
Ba	100	130	85	140	250
La	7.3	7.0	3.7	6.0	7.0
Ce	15	16	4.5	11	16
Nd	12	9	5	8	10
Sm	2.4	2.32	1.07	2.0	2.0
Eu	0.47	0.49	0.23	0.35	0.57
Tb	0.40	0.38	0.17	0.28	0.30
Dy	1.9	2.3	1.5	1.9	2.0
Yb	0.84	0.93	0.52	0.84	1.16
Lu	0.13	0.15	0.11	0.13	0.16
Hf	2.0	2.0	1.5	1.8	2.9
Th	–	<0.2	–	<0.5	<1.0

[a] In ppm, except for Na, Ti, and Fe; uncertainties as in Table 2

Average microprobe analyses of olivine phenocryst rims and cores and xenocryst cores in Col 11 and 13, and of remnant, xenocrystic olivines in Col 9 and 17 are listed in Table 15. Total variation in the olivine compositions is less than 18 mol% Mg_2SiO_4 in a single sample. Differences between average phenocryst rims and cores in Col 11 and 13 are less than 3 mol% (Mg). Phenocrysts are normally zoned in both samples. Cores of reacting xenocrysts are considerably more magnesian than phenocrysts. The neutron activation analysis of a hand picked olivine separate from Col 11 is listed in Table 14.

Fe–Ti Oxides

Titanomagnetite is common in all samples (1) as isolated microphenocrysts and phenocrysts up to 1.0 mm i.d., (2) as inclusions within the rims of pyroxenes and occassionally within plagioclase, olivine, and hornblende, (3) within hornblende reaction rims, and (4) as abundant groundmass microcrystals. Hematite-ilmenite solid solutions are extremely rare, owing to the low TiO_2 contents (0.60–0.79 wt.%) of these andesites. In Col 9, a small cluster of hematite-ilmenite crystals was analyzed. A single, but often variable population of titanomagnetite is present in the hornblende-andesite samples. Titanomagnetite compositions in these samples could not be consistently related to textural groupings. In the olivine-andesites, however, titanomagnetites included within olivine phenocrysts are enriched in Al, Cr, and Mg, and depleted in Ti, V, Fe, Mn, and Ca compared with other titanomagnetites in these samples.

Average microprobe analyses for titanomagnetites, including two populations in the olivine-andesites, and for hematite-ilmenite in Col 9 are listed in Table 16 in order of increasing sample age. The analyses have been recalculated for ferric iron after the method of Carmichael (1967). Neutron activation analyses of hand picked titanomagnetite separates from five samples are listed in Table 17. Titanomagnetite in Col 11 and Col 13 is very fine grained and restricted to the groundmass. Consequently, the Col 11 separate is impure, as attested to by its high Na content.

Table 18. Ranges of weight fraction distribution coefficients

	plag	opx	cpx	hbd	oliv	titanmt
Sc	0.01 – 0.03	2.2 – 4.7	6.9 – 16	8.1 –13	0.30	1.7 – 3.3
V	0.07 – <0.47	0.47– 2.2	1.1 – 5.2	6.3 –13	0.08	8.7 – 54
Cr	0.02 – <0.25	21 –143	43 –245	31 –90	34	93 –340
Ni	<0.06 – >0.61	>0.79– 24	>4.6 – 9.0	7.2 –16	58	9.6 – 19
Zn	0.13 – 0.25	2.6 – 4.4	6.5 – 12	5.0 – 8.7	1.5	5.4 – 13
Cs	0.04 – <0.31	<0.31– 0.45	<0.17– 0.64	<0.15– 0.50	<0.27	<0.39– <0.63
Ba	0.08 – 0.36	0.03– 0.23	0.02– 0.05	0.15– 0.22	<0.02	0.12– 0.40
La	0.13 – 0.21	<0.03– 0.30	0.14– 0.23	0.14– 0.19	<0.02	0.22– 0.45
Ce	0.12 – 0.18	<0.02– 0.33	0.20– 0.36	0.29– 0.37	<0.01	0.12– 0.42
Nd	0.08 – 0.16	0.05– 0.43	0.44– 0.70	0.70– 0.95	<0.02	0.25– 0.55
Sm	0.07 – 0.10	0.06– 0.43	0.78– 1.3	1.2 – 1.7	0.01	0.29– 0.55
Eu	0.36 – 0.73	0.07– 0.42	0.72– 1.2	1.5 – 1.9	<0.03	0.22– 0.42
Tb	0.05 – 0.08	0.15– 0.48	1.1 – 2.0	1.5 – 2.5	<0.11	0.37– 0.67
Dy	<0.03 – 0.09	0.21– 0.56	1.2 – 1.9	1.7 – 2.5	<0.10	0.44– 0.58
Yb	0.01 – 0.02	0.29– 0.56	0.93– 1.4	1.1 – 1.6	0.03	0.24– 0.47
Lu	<0.05 – <0.10	0.31– 0.68	0.86– 1.4	1.0 – 1.6	<0.08	0.32– 0.44
Hf	0.01 – 0.02	<0.02– 0.22	0.21– 0.34	0.34– 0.52	<0.02	0.30– 0.62
Th	0.004– <0.013	0.04– 0.22	<0.04– <0.16	<0.13– 0.25	<0.02	<0.05– <0.42

Distribution coefficients are calculated by dividing the concentration of an element in the crystal separate by that in the groundmass separate. High and low values are reported for each element. Only a single olivine separate was analyzed

Distribution Coefficients

Weight fraction distribution coefficients (K_D's) governing the partitioning of trace elements between melt and crystalline phases can be readily calculated from the neutron activation data in Tables 5, 8, 10, 12, 14, and 17. Ranges of K_D's for each element in each analyzed phase of the suite are tabulated in Table 18. The listed olivine and plagioclase K_D's compare favorably with those compiled by Arth, (1976) for andesites and basalts. Pyroxene and hornblende K_D's for rare earth elements generally range higher in the Colima samples. The K_D's for Ba are higher in Colima's orthopyroxenes, but lower in the hornblendes than those of Arth's compilation. Because they account for the presence of important included phases, such as apatite, in the analyzed minerals, distribution coefficients determined from naturally occurring crystal-groundmass pairs may most realistically represent actual operative magmatic values.

Estimation of Intensive Variables

Lithostatic Pressure

Of all the important intensive magmatic variables, lithostatic pressure is one of the most difficult to accurately estimate on the basis of phase equilibria. No reliable geobarometer is currently available for application to Colima's post-caldera andesites. There are, however, geologic constraints on the pressures of phase equilibria. The summit calderas at Volcán Colima and many other major composite volcanoes undoubtedly record earlier voluminous eruptions which significantly drained large magma chambers within or just below the volcanic piles. The majority of crystalline phases in calc-alkaline andesites probably precipitate in such subvolcanic magma chambers (Anderson, 1976; Marsh, 1976). Phenocryst rims and microphenocrysts in Colima's andesites are believed to have crystallized within the upper levels of the volcanic system, just before or during eruption. The equilibration pressure of the phenocryst assemblage in Col 11 has been calculated as 1,000 bars (Ghiorso and Carmichael, 1979), but the errors of the calculation are large. Consequently, calculations involving coexisting phenocryst rim compositions are performed at assumed lithostatic pressures of 100, 1,000, and 2,000 bars. Assuming an average density of 2.6 g/cm^3 for the volcanic pile, the pressure at the base of the pile, 3 km below the summit is equal to 765 bars.

Temperature

Table 20 lists pre-eruptive temperature estimates for Colima's post-caldera andesites derived from a variety of geothermometers. A brief discussion of each geothermometer follows. Plagioclase/liquid geothermometry will be discussed later in an evaluation of magmatic water contents.

Fe–Ti Oxide Geothermometry – Buddington and Lindsley's (1964) Fe–Ti oxide geothermometer is probably the most precise method presently available for estimating magmatic temperatures and oxygen fugacities (Wright and Weiblen, 1968; Helz, 1973; Ulmer et al., 1976). Titanomagnetite is present in all investigated post-caldera samples from Volcán Co-

lima, but owing to the low TiO_2 contents of these andesites (0.60–0.79 wt.%), hematite-ilmenite is extremely rare. The only reliable analysis for this phase was obtained for Col 9, the most recent of the samples. Following the recalculation procedures discussed in Carmichael (1967), an equilibration temperature of 986° C and oxygen fugacity of $10^{-9.31}$ were calculated for Col 9. Because of the extreme scarcity of hematite-ilmenite, these values are considered somewhat unreliable.

Pyroxene Geothermometery – Wood and Banno (1973) formulated a geothermometer based on the shape of the orthopyroxene-clinopyroxene miscibility gap for natural, iron-bearing systems. The geothermometer was later recalibrated by Wells (1977) using a larger body of experimental data. Both of the geothermometers were applied to the samples investigated in this study. Temperatures were calculated from phenocryst rim compositions, which presumably record magmatic temperatures on eruption. They range from 963°–1,023° C in the hornblende-andesites and from 1,017°–1,056° C in the olivine-andesites.

Oxygen Isotope Geothermometry – Hand picked mineral and groundmass separates from Col 9, 15, and 11 were kindly analyzed for O^{18}/O^{16} by K. Kyser working with J. O'Neil at the USGS in Menlo Park, California. The data are tabulated in Table 19. Anderson et al. (1971) formulated a magmatic geothermometer based on the partitioning of oxygen isotopes between plagioclase and magnetite. Kyser et al. (1980) calibrated four other isotopic exchange geothermometers based on the distribution of oxygen isotopes between coexisting phenocrysts and/or glass. Temperatures derived from each of these geothermometers are listed in Table 20.

Crystal-Melt Geothermometers – Ghiorso and Carmichael (1979) recently formulated a crystal-liquid equilibrium solution model based on experimentally equilibrated plagioclase-melt and olivine-melt pairs. Compositions of plagioclase rim-groundmass pairs for Colima's hornblende-andesites were used to solve for T-wt.% H_2O values at 1 and 3 kb pressure (Table 20). As discussed in Ghiorso and Carmichael (1979) the presence of olivine in Col 11 allows determination of a unique $T-P$-wt.% H_2O point for

Table 19. O^{18}/O^{16} Ratios in mineral and groundmass separates

Col	plag	cpx	opx	mt	hbd	oliv	grdm
9	6.4	5.4	6.1	3.3	–	–	6.9
15	6.4	5.5	5.5	4.0	6.7	–	5.7
11	6.8	5.7	6.1	–	–	5.7	6.5

As discussed in the text, the groundmass of Col 15 appears to be out of chemical and isotopic equilibrium with the crystals
Analytical uncertainties (+/−0.1‰)

Table 20. Temperature estimations for Colima's post-caldera andesites (° C)

Col	Ta	T1	T2	T3	T4	T5	T6	T7	T8	T9
9	940	986	992	968	882	–	–	880	1,020	1,021 (2.2) 986 (3.4)
6	940	–	995	974	–	–	–	–	–	987 (3.2) 970 (4.3)
17	940	–	995	977	–	–	–	–	–	952 (4.6) –
15	1,000	–	1,023	1,010	1,028	–	–	1,200	1,200	1,192 (0.2) 1,175 (0.4)
18	940	–	976	971	–	–	–	–	–	– –
2	940	–	971	963	–	–	–	–	–	1,052 (2.5) 1,022 (3.8)
7	940	–	984	971	–	–	–	–	–	1,077 (1.9) 1,047 (3.2)
11	1,030	–	1,017	1,018	–	1,130	1,150	1,030	1,140	1,120 (0.8)
13	1,060	–	1,056	1,053	–	–	–	–	–	–

Ta: Assumed pre-eruptive temperature
T1: Fe–Ti oxides (Buddington and Lindsley, 1964)
T2: Pyroxene phenocryst rims (Wells, 1977)
T3: Pyroxene phenocryst rims (Wood and Banno, 1973)
T4: O^{18}/O^{16} plag-mt (Anderson et al., 1971)
T5: O^{18}/O^{16} gl-oliv (Kyser et al., 1980)
T6: O^{18}/O^{16} cpx-oliv (Kyser et al., 1980)
T7: O^{18}/O^{16} cpx-gl (Kyser et al., 1980)
T8: O^{18}/O^{16} opx-gl (Kyser et al., 1980)
T9: Intersections of albite and anorthite components at 1 and 3 kb in T-%H_2O space (Ghiorso and Carmichael, 1979)
Numbers in parentheses are wt.% H_2O

equilibration of phenocryst rims of 1,120° C, 1 kb, and 0.8% H_2O.

For the sake of subsequent thermodynamic calculations in which temperature is a variable, it is desirable to appraise the relative merits of the temperature estimates in Table 20 and to choose a single value for each sample. In the case of the hornblende-andesites, this process is greatly facilitated by knowledge of the experimentally determined stability field of hornblende.

The stability of hornblende in andesites and basalts has been investigated experimentally by a variety of workers (Eggler, 1972a and b; Eggler and Burnham, 1973; Allen et al., 1975; Stern et al., 1975; Allen and Boettcher, 1978). The upper temperature stability limit of hornblende decreases with increasing silica content of the liquid from 1,050° C in basalts with 50 wt.% SiO_2 to 940°–970° C in andesites with 59 wt.% SiO_2. Accordingly, pre-eruptive temperatures in Colima's post-caldera hornblende andesites with 60%–62% SiO_2 (Col 9, 6, 17, 18, 2, and 7) are assumed to be 940° C. Estimates for these samples listed in Table 20 range from 880°–1,080° C. For Col 15 (57.6% SiO_2), temperatures calculated from solid equilibria, both elemental and isotopic, range from 1,010°–1,028° C. Liquid-solid geothermometer of both types predict anomalously high temperatures for the hornblende-bearing Col 15 of 1,175°–1,200° C. The groundmass glass of the 1913 scoria Col 15 appears to be out of chemical and isotopic equilibrium with the crystalline phases. A pre-eruptive temperature of 1,000° C is assumed for Col 15. Estimates for the olivine andesites Col 11 and 13 range from 1,017°–1,150° C and 1,053°–1,056° C respectively. Pre-eruptive temperatures of 1,030° C and 1,060° C are assumed for these samples. The assumed values of pre-eruptive temperature are also listed in Table 20. The choices are admittedly somewhat arbitrary, but we are confident in the relative trend of the assumed temperatures.

Oxygen Fugacity

A single estimate of oxygen fugacity equal to $10^{-9.31}$ at 986° C was obtained from the coexisting Fe–Ti oxide phases of Col 9 using the geothermometer of Buddington and Lindsley (1964). In the olivine andesites (Col 11 and 13), orthopyroxene, olivine, and titanomagnetite were all stable pre-eruptive phases. Equation (1) can, therefore, be solved for pre-eruptive f_{O_2} at assumed lithostatic pressures of equilibration.

$$\underset{\text{oliv}}{6Mg_2SiO_4} + \underset{\text{opx}}{6FeSiO_3} + \underset{\text{gas}}{O_2} = \underset{\text{titanmt}}{2Fe_3O_4} + \underset{\text{opx}}{12MgSiO_3} \quad (1)$$

Thermodynamic calculations in this paper were performed by fitting log K of each reaction between 900° and 1,100° C to an equation of the form $\log K = A/T + B + C(P-1)/T$ using the thermodynamic data of Helgeson et al. (1978) and Ghiorso and Carmichael (1979). Coefficients for each reaction are listed in Table 21. Equation 1 was solved at temperautes listed in Table 20 and pressures of 100 and 1,000 bars, using activities of $MgSiO_3$, $FeSiO_3$, and Mg_2SiO_4 calculated from phenocryst rim compositions listed in Tables 9 and 15. and activities of Fe_3O_4 calculated from titanomagnetite compositions listed in Table 16. ΔV_{solids} for the reaction is small and calculated values of pre-eruptive f_{O_2} are only weakly dependent on assumed pressures of equilibration.

Col	T (°K)	P (bars)	$\log f_{O_2}$
11	1,303	100	−8.32
		1,000	−8.30
13	1,333	100	−7.83
		1,000	−7.81

Pre-eruptive T–f_{O_2} points calculated for Col 9 from Fe–Ti oxide geothermometry and for Col 11 and

Table 21. Coefficients A, B, and C from the equation $\log K = A/T + B + C(P-1)/T$ for the listed reactions

Equation	Reaction	A	B	C
1	$\underset{\text{oliv}}{6Mg_2SiO_4} + \underset{\text{opx}}{6FeSiO_3} + \underset{\text{gas}}{O_2} = \underset{\text{titanmt}}{2Fe_3O_4} + \underset{\text{opx}}{12MgSiO_3}$	27,081	−8.874	−0.20
3	$\underset{\text{opx}}{FeSiO_3} + 1/6\underset{\text{gas}}{O_2} = 1/3\underset{\text{titanmt}}{Fe_3O_4} + \underset{\text{liquid}}{SiO_2}$	3,916	−1.130	−0.114
4	$\underset{\text{titanmt}}{1/3Fe_3O_4} + \underset{\text{hbd}}{Mg_7Si_8O_{22}(OH)_2} = \underset{\text{opx}}{7MgSiO_3} + \underset{\text{opx}}{FeSiO_3} + \underset{\text{gas}}{1/6O_2} + \underset{\text{gas}}{H_2O}$	−8,603	8.650	0.142

Coefficients A and B were determined by fitting log K of each reaction at 1 bar pressure and temperatures between 900° and 1,100° C
Thermodynamic data is taken from Helgeson et al. (1978) except for SiO_2 liquid which is taken from Ghiorso and Carmichael, (1979)

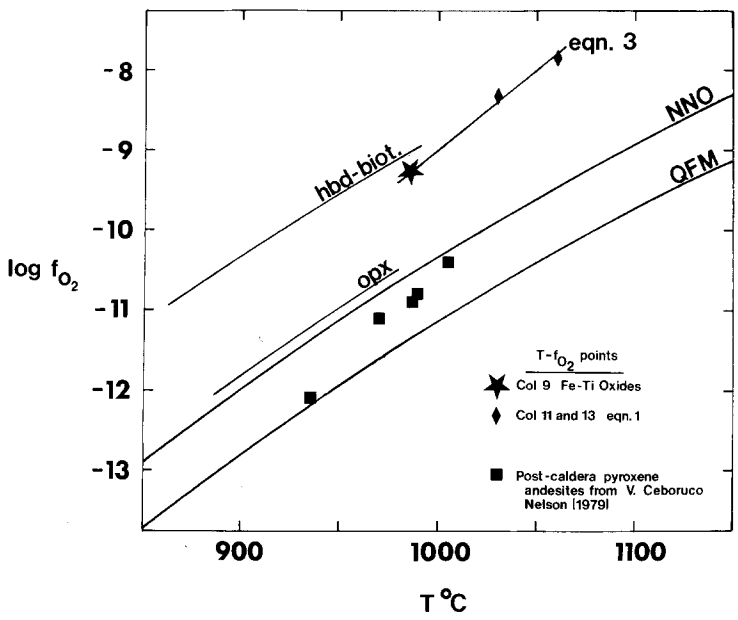

Fig. 7. T-f_{O_2} plot including data points for *post-caldera andesites* from V. Colima derived from Fe–Ti oxide compositions and solution of Eq. (1), and data points for *post-caldera pyroxene andesites* from V. Ceboruco (Neson, 1979) derived from *Fe–Ti oxide* compositions. *Hbd-biot* and *opx* curves were taken from Carmichael (1967). Eq. (2) is a best fit line through the upper three data points

13 from solution of Eq. (1) are plotted on Fig. 7. The three points lie 1.2–1.6 log units above the NNO buffer, near the extrapolation of the curve for siliceous magmas containing biotite and amphibole phenocrysts in the absence of orthopyroxene (Carmichael and Ghiorso, 1980).

Fudali (1965) experimentally determined oxygen fugacities in an olivine basalt, an olivine andesite, and two pyroxene andesites from the Mt. Hood area, by reproducing naturally occurring Fe^{+3}/Fe^{+2} ratios at 1,200° C. Determined values of f_{O_2} ranged from $10^{-8.5}-10^{-7}$, straddling the NNO buffer by approximately 0.7 log units. A nearly identical $T-f_{O_2}$ relationship ($\log f_{O_2}=$NNO $+/-$ 0.7) was calculated by Nelson (1979) for andesites from Volcán Ceboruco using Buddington and Lindsley's (1964) Fe–Ti oxide geothermometer. $T-f_{O_2}$ points for post-caldera pyroxene andesites from V. Ceboruco are also included in Fig. 7. The NNO buffer is essentially coincident with the curve for siliceous magmas containing orthopyroxene phenocrysts (Carmichael and Ghiorso, 1980).

The relative positions of $T-f_{O_2}$ trends for hornblende-andesites from V. Colima and pyroxene-andesites from V. Ceboruco on Fig. 7 are supported by a comparison of whole rock $Fe_2O_3/FeO+Fe_2O_3$ ratios. Values for Colima's post-caldera andesites range from 0.33–0.42 and are consistently higher than those from Ceboruco's andesites (0.21–0.25; Nelson, 1979). As discussed by Carmichael and Nicholls (1967), Fe^{+3}/Fe^{+2} ratios in silicate melts are direct functions of alkali content, f_{O_2}, and $1/T$. Available geothermometers record similar pre-eruptive temperatures for andesites from the two volcanoes. Because Ceboruco's andesites are more alkalic, it must be concluded that f_{O_2} was significantly higher in Colima's magmas (Luhr and Nelson, 1979). In this paper it is assumed that Colima's magmas are buffered in $T-f_{O_2}$ space along the line through the three data points in Fig. 7, whereby:

$$\log f_{O_2}=-35.66+0.0209\ (T\ ^\circ\mathrm{K}). \tag{2}$$

This relationship is used in all subsequent calculations on Colima's magmas. It is not greatly dependent on the assumed temperatures for the olivine andesites.

Silica Activity

Each of the investigated andesites contains coexisting orthopyroxene and titanomagnetite crystals, and if a lithostatic pressure of equilibration is assumed, Eq. (3) can be solved for the activity of silica in the coexisting melt phase.

$$\underset{\text{opx}}{FeSiO_3}+\underset{\text{gas}}{1/6O_2}=\underset{\text{titanmt}}{1/3Fe_3O_4}+\underset{\text{melt}}{SiO_2}. \tag{3}$$

Reaction coefficients for Eq. (3) are listed in Table 21. The calculations were performed using $FeSiO_3$ and Fe_3O_4 activities for orthopyroxene rim and titanomagnetite compositions (Tables 9 and 16), oxygen fugacities as calculated from Eq. (2), and assumed pressures for pre-eruptive equilibration of 100 and 1,000 bars. The results of the calculations are listed in Table 22. At 100 bars pressure, calculated values of $a_{SiO_2}^{melt}$ range from 0.65–0.74. As indicated, the calcu-

Table 22. Calculated silica activities

Col	Eq. 4			Ghiorso and Carmichael (1980)		
	T (° K)	P (bars)	$a_{SiO_2}^{melt}$	T (° K)	P (bars)	$a_{SiO_2}^{melt}$
9	1,213	100	0.71	1,294	1,000	0.72
		1,000	0.59			
6	1,213	100	0.71	1,260	1,000	0.74
		1,000	0.59			
17	1,213	100	0.69	1,225	1,000	0.75
		1,000	0.58			
15	1,273	100	0.71	1,465	1,000	0.61
		1,000	0.65			
18	1,213	100	0.65	–	–	–
		1,000	0.59			
2	1,213	100	0.65	1,325	1,000	0.71
		1,000	0.54			
7	1,213	100	0.68	1,350	1,000	0.71
		1,000	0.56			
11	1,303	100	0.72	1,393	1,000	0.60
		1,000	0.68			
13	1,333	100	0.74	–	–	–
		1,000	0.69			

lation is strongly dependent on assumed equilibration pressure. At any value of P, however, $a_{SiO_2}^{melt}$ is higher for the three andesites of the most recent eruptive cycle (Col 9, 6, and 17), versus earlier hornblende-andesites of similar bulk composition (Col 18, 2, and 7).

Values of $a_{SiO_2}^{melt}$ were also calculated from analyzed groundmass compositions at $P=1$ kb as discussed in Ghiorso and Carmichael (1979). These values and the calculated temperatures are listed in Table 22. Silica activities calculated by this method are also higher for Col 9, 6, and 17 than for the earlier, compositionally similar Col 7 and 2. The significance of this observation is discussed later in this section in relation to other peculiarities of the fourth cycle andesites.

Water Fugacity and Water Content

Two methods of calculating magmatic water pressure can be applied to Colima's post-caldera andesites. The first is based on the empirical plagioclase geothermometers of Kudo and Weill (1970) and Drake (1976), and the second is based on thermodynamic calculation.

Plagioclase geothermometers are dependent on coexisting plagioclase and silicate melt compositions, and on the water pressure in the system. Given an analysis of a coexisting plagioclase-melt pair and an independent estimate of equilibration temperature,

Table 23. Calculation of P_{H_2O} from plagioclase geothermometry

Col	9	6	17	15	2	7	11
T(° C)	940	940	940	1,000	940	940	1,030
P_{H_2O} (b.)	1,750	1,750	1,800	2,100	2,400	2,150	1,900

Water pressures calculated from the plagioclase geothermometers of Kudo and Weill (1970) and Drake (1976) using assumed pre-eruptive temperatures

plagioclase geothermometers can be used to predict P_{H_2O} (Stormer and Carmichael, 1970). Groundmass separates from seven of Colima's post-caldera andesites have been wet chemically analyzed (Table 4). An estimate for pre-eruptive water pressure in these magmas was obtained by determining the value of P_{H_2O} which is necessary to bring the temperature calculated from plagioclase phenocryst rim-groundmass pairs into harmony with the assumed value for pre-eruptive temperature. Calculated values of P_{H_2O}, which range from 1,750–2,400 bars, are listed in Table 23. The lowest values of P_{H_2O} are recorded for the three samples of the most recent eruptive cycle (Col 9, 6, and 17).

Analyses of coexisting hornblende, orthopyroxene, and titanomagnetite in six of Colima's post-caldera andesites (no hornblende analysis was obtained for Col 9) allow solution of Eq. (4) for water fugacity at assumed values for lithostatic pressure of equilibration. Reaction coefficients for Eq. (4) are listed in Table 21.

$$\underset{\text{titanmt}}{1/3\,Fe_3O_4} + \underset{\text{hbd}}{Mg_7Si_8O_{22}(OH)_2} = \underset{\text{opx}}{7\,MgSiO_3} + \underset{\text{opx}}{FeSiO_3} + \underset{\text{gas}}{1/6\,O_2} + \underset{\text{gas}}{H_2O}. \quad (4)$$

Since no thermodynamic data exists for monoclinic $Mg_7Si_8O_{22}(OH)_2$ (cummingtonite), data for the orthorhombic variety (anthophyllite) have been used. The difference in heat of formation of the two forms should only be a few hundred calories. The greatest uncertainty in the calculation of $f_{H_2O}^{vap}$ by this method lies in the determination of the activity of $Mg_7Si_8O_{22}(OH)_2$ in the hornblende. Powell (1975) formulated a regular solution model for activity-composition relations in hornblendes based on coexisting cummingonite-hornblende pairs in a suite of New Zealand rhyolites, which record Fe–Ti oxide quench temperatures of 725°–755° C. Using a_{cumm}^{hbd} values calculated from Powell's model, Eq. (4) predicts values of pre-eruptive water fugacity in Colima's andesites that are considered unrealistically high, 3–4 kb. The

Table 24. Calculation of magmatic water content

Col	T °C	T °K	P (bars)	$\gamma^{hbd}_{cumm}=31$					$\gamma^{hbd}_{cumm}=96$				
				$f^{melt}_{H_2O}$ (b)	$P^{melt}_{H_2O}$ (b)	$X^{melt}_{H_2O}$	wt.%$^{melt}_{H_2O}$	wt.%$^{magma}_{H_2O}$	$f^{melt}_{H_2O}$ (b)	$P^{melt}_{H_2O}$ (b)	$X^{melt}_{H_2O}$	wt.%$^{melt}_{H_2O}$	wt.%$^{magma}_{H_2O}$
6	940	1,213	100	192	191	0.080	2.2	1.2	594	591	0.141	4.1	2.2
			1,000	244	225	0.081	2.2	1.2	757	697	0.142	4.1	2.2
			2,000	320	288	0.082	2.3	1.2	991	893	0.144	4.2	2.3
17	940	1,213	100	206	205	0.083	2.3	1.0	637	634	0.146	4.3	1.9
			1,000	262	241	0.083	2.3	1.1	811	746	0.147	4.3	1.9
			2,000	344	310	0.085	2.4	1.1	1,062	957	0.149	4.4	2.0
15	1,000	1,273	100	299	297	0.095	2.7	1.9	925	923	0.166	5.0	3.4
			1,000	377	354	0.095	2.7	1.9	1,167	1,097	0.167	5.0	3.4
			2,000	486	455	0.096	2.7	1.9	1,507	1,564	0.168	5.0	3.5
18	940	1,213	100	376	374	0.112	3.2	2.0	1,161	1,155	0.197	6.0	3.6
			1,000	479	441	0.113	3.2	2.0	1,479	1,361	0.198	6.1	3.6
			2,000	627	565	0.115	3.3	2.0	1,936	1,745	0.202	6.2	3.6
2	940	1,213	100	225	224	0.087	2.4	1.6	697	693	0.153	4.5	3.0
			1,000	286	263	0.087	2.4	1.6	887	816	0.154	4.5	3.0
			2,000	375	338	0.089	2.5	1.7	1,161	1,046	0.156	4.6	3.0
7	940	1,213	100	248	247	0.091	2.6	1.6	769	765	0.160	4.8	3.0
			1,000	316	291	0.092	2.6	1.6	979	901	0.161	4.8	3.0
			2,000	414	373	0.093	2.6	1.7	1,282	1,155	0.164	4.9	3.1

$P^{melt}_{H_2O}$ is calculated from values of $f^{melt}_{H_2O}$ and fugacity coefficients listed in Burnham et al. (1969)

major problem probably lies in trying to apply Powell's model outside of the compositional and temperature ranges of its formulation. Allen and Boettcher (1978) recently published analyses of two coexisting orthopyroxene-hornblende pairs from experiments on a Mt. Hood andesite at 13 kb, 900° C, and $X^{vap}_{H_2O}=0.75$, and 13 kb, 940° C, and $X^{vap}_{H_2O}=0.50$, with f_{O_2} buffered along HM. An unanalyzed opaque mineral, undoubtedly titanomagnetite, was reported in both runs. Converting $X^{vap}_{H_2O}$ to $f^{vap}_{H_2O}$ using the modified Redlich-Kwong equation of Flowers (1979), formulating X^{hbd}_{cumm}, a^{opx}_{en}, and a^{opx}_{fs} from the reported analyses as discussed in Tables 13 and 9, and assuming $a_{mt}=0.75$ in both runs, which has only a small effect on the calculation, Eq. (4) was solved for the activity coefficient of cummingtonite in hornblende for the two experimental runs. The calculated values are $\gamma^{hbd}_{cumm}=96$ and 31, for the 900° and 940° runs respectively. These extracted activity coefficients have been multiplied by values of X^{hbd}_{cumm} listed in Table 13 to derive two estimates for a^{hbd}_{cumm} in each sample. Equation (4) was then solved for $f^{vap}_{H_2O}$ using component activities calculated from orthopyroxene rim and titanomagnetite compositions at assumed lithostatic pressures of equilibration of 100, 1,000, and 2,000 bars. Values of $f^{vap}_{H_2O}$ can be converted to mole fractions of H_2O in the melt phase ($X^{melt}_{H_2O}$) and ultimately to wt.% H_2O in the melt as discussed by Carmichael et al. (1977). An average gram formula weight of 69, determined for the groundmass composition of the hornblende andesites was used in the calculation. Pre-eruptive water contents for the magmas (whole rock) can then be determined by weighting the water contents of the melt phase and hornblende crystals by the volume fractions of groundmass and hornblende in each sample (Table 6). Values of pre-eruptive $f^{vap}_{H_2O}$, $P^{vap}_{H_2O}$, $X^{melt}_{H_2O}$, wt.% H_2O in melt (groundmass), and wt.% H_2O in magma (whole rock) calculated for $P_{lith}=100$, 1,000, and 2,000 bars, and $\gamma^{hbd}_{cumm}=96$ and 31 are listed in Table 24.

Values of f_{H_2O} calculated from Eq. (4) are strongly dependent on assumed lithostatic pressures. Conversion to $X^{melt}_{H_2O}$ (Carmichael et al., 1977) has a similar, opposing pressure dependency, however, resulting in wt.% H_2O values that are only weakly dependent on assumed pressure. Estimates of pre-eruptive magmatic water content in Colima's post-caldera hornblende-andesites range from 1.0–3.6 wt.% as listed in Table 24. At present, this method of calculation is probably only suitable for estimates of relative, not absolute magmatic water contents.

Values of P_{H_2O} determined from plagioclase geothermometry (Table 23). are somewhat higher than water pressures calculated from Eq. (4) at $P_{lith}=2{,}000$ bars and $\gamma^{hbd}_{cumm}=96$ (Table 24). This discrepancy may be due to the fact that plagioclase-melt equilibria experiments were conducted at $P_{H_2O}=P_{Total}$. At undersaturated conditions, which probably apply in

most natural magmas, these two variables have opposing influences on plagioclase-melt equilibria. Despite absolute differences in calculated water contents, both the plagioclase geothermometers and Eq. (4) predict the same relative trends, with the lowest, pre-eruptive water pressures for Col 6 and 17, samples from the most recent eruptive cycle. As indicated in Table 24, the calculated magmatic water contents of these samples are 0.4–1.7 wt.% lower than those of earlier hornblende-andesites. The consistency of the two methods of calculation encourages us in the interpretation that magmatic water content has been significantly reduced during the most recent eruptive cycle.

Andesites of the Fourth Eruptive Cycle

The third eruptive cycle at Volcán Colima began in 1869 with the eruption of hornblende-rich block lavas. Col 2 and 18 were sampled from these flows and record the highest pre-eruptive water contents in the post-caldera suite (Tables 23 and 24). The third cycle ended in 1913 with a voluminous ashflow eruption of hornblende-rich andesite (Col 15), also recording a high water content.

The three investigated andesites which erupted since 1961, during the most recent eruptive cycle (Col 9, 6, and 17), display a number of peculiarities relative to earlier hornblende-andesites of nearly identical bulk composition (Col 18, 2, and 7). These include: (1) lower hornblende contents (0.6–1.0% vs 1.7–5.0%), (2) higher total crystal contents (47.2–51.6% vs 35.8–38.7%), (3) higher pre-eruptive silica activities as calculated from Eq. (3) (0.69–0.71 vs 0.65–0.68; assuming $P_{\text{lith}}=100$ bars), (4) lower pre-eruptive magmatic water contents as calculated from Eq. (4) (1.9–2.2% vs 3.0–3.6%; assuming $P_{\text{lith}}=$ 100 bars and $\gamma_{\text{cumm}}^{\text{hbd}}=96$), and (5) relatively iron rich rims on orthopyoxenes. All of these observations are thought to be consistent with the interpretation that andesites of the fourth eruptive cycle were significantly less hydrous than earlier post-caldera andesites of similar bulk composition. The highly energetic ashflow eruption of 1913 (Waitz, 1915), which closed the third eruptive cycle, may have triggered this transition by depleting Colima's magma system in volatiles. At constant bulk composition and temperature, less hydrous magmas will have higher solidus temperatures, and thus, higher crystal contents. Silica activity was higher in the fourth cycle andesites as the combined result of higher crystal contents leading to more siliceous groundmasses (Table 4) and of lower water contents. Water acts to decrease polymerization in silicate melts and lower water contents cause higher activities of silica. The lack of slight Mg-rich rims on orthopyroxenes in the fourth cycle andesites is also interpreted as consistent with relatively lower water contents, as discussed in the next section.

Mineral Zoning and Textural Patterns

A characteristic feature of calc-alkaline andesites is their textural complexity, often accompanied by complex mineralogical zoning patterns. In Colima's post-caldera andesites, the most striking mineral zoning and textural features are the Mg-rich rims on pre-1961 pyroxenes and the brown glass inclusion zones within plagioclase phenocrysts. The same phenomena have been reported in the literature from a wide spectrum of calc-alkaline provinces (Kuno, 1936, 1950; MacDonald and Katsura, 1965; Eichelberger, 1975, 1978; Anderson, 1976; Johnston, 1978; Sakuyama, 1979).

Using optical methods, Kuno (1936) identified relatively Mg-rich rims on pyroxenes and clear, relatively Ca-rich rims on glass inclusion riddled plagioclase cores in the pigeonite-bearing andesites from Hakone Volcano, Japan. The observation that all phenocrystic phases in these andesites posess higher temperature rims than cores led Kuno to invoke a pre-eruptive mixing event involving a dacitic magma and a hotter andesitic magma. Phenocryst cores were thought to have crystallized in the cooler dacitic end member; the andesitic magma was presumably crystal free. Most subsequent investigations cited above have supported Kuno's early interpretations. Following crystal growth rate studies by Lofgren et al. (1974, 1975) and Donaldson et al. (1975), however, petrologists recognized similarities between glass inclusions incorporated by skeletal crystals grown under supercooled conditions and many glass inclusions in natural crystals (Gutmann, 1977; Dungan and Rhodes, 1978; Evans and Nash, 1979; Rhodes et al., 1979). Dungan and Rhodes (1978) outlined criteria for distinguishing resorption from primary growth inclusions.

Olivine-Andesites

The most pronounced Mg-rich pyroxene rims and clear rims on glass inclusion riddled plagioclase cores in Colima's post-caldera suite occur in the olivine andesites, Col 11 and 13. It might be suggested that both of these rim phenomena occurred on eruption in a manner analogous to the hornblende reaction rims. Both phenomena are observed in the quickly

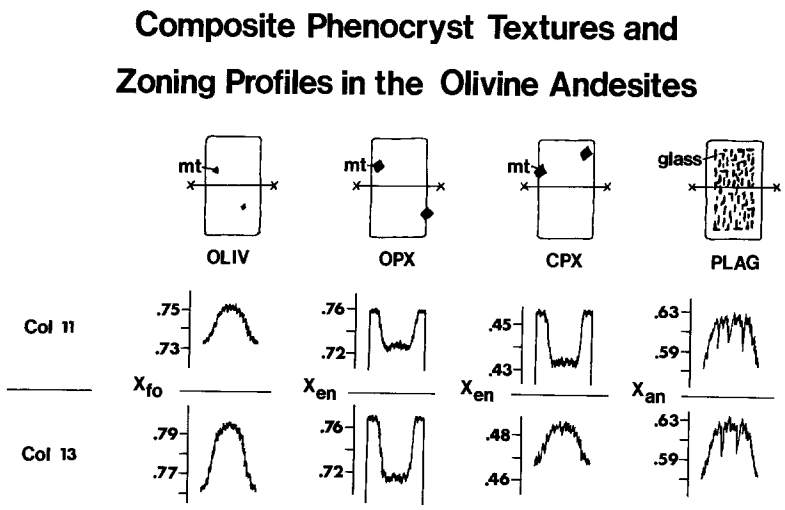

Fig. 8. Idealized *phenocryst textures* and *zoning profiles* in the major silicate phases of the *olivine-andesites Col 11 and 13*

quenched scoria of Col 15, however, whose hornblende does not show reaction rims, demonstrating that the anomalous pyroxene and plagioclase rims record pre-eruptive conditions. Idealized zoning profiles for the four major phases in Col 11 and 13 are shown in Fig. 8. As mentioned previously, olivine and plagioclase phenocrysts in both samples and most clinopyroxenes in Col 13 are normally zoned, while most orthopyroxene phenocrysts of both samples and clinopyroxenes of Col 11 are reversely zoned, with thin, Mg-rich rims.

In an experimental study of equilibria between olivine and basaltic liquids, Roeder and Emslie (1970) suggested that the distribution coefficient for partitioning of ferrous iron and magnesium between olivine and liquid, $K_D = X^{oliv}_{FeO} X^{liq}_{MgO} X^{oliv}_{MgO} X^{liq}_{FeO}$, is equal to 0.30 and is essentially independent of temperature. Combining their data with that of Medaris (1969) and Williams and Eugster (1969) on the partitioning of Fe^{+2}-Mg between orthopyroxene and olivine, they also calculated a distribution coefficient for Fe^{+2}-Mg partitioning between orthopyroxene and liquid of 0.23, similarly independent of temperature. These relationships can be used to demonstrate the presence or absence of equilibrium between coexisting orthopyroxene and olivine crystals, and for complexly zoned crystals, they can be used to determine whether or not these two phases have maintained equilibrium throughout the crystallization interval (Johnston, 1978). Values of X_{FeO}/X_{MgO} in the liquid predicted by the above expressions for equilibrium with olivine and orthopyroxene phenocryst rim and core compositions in Col 11 and 13 are listed below. The liquid values predicted by olivine and orthopyroxene rim compositions are nearly identical in both samples, suggesting that the rims of these phases crystallized in equilibrium. The phenocryst core compositions,

	phen. rims		phen. cores	
	oliv	opx	oliv	opx
Col 11	1.21	1.25	1.11	1.48
Col 13	1.05	1.15	0.87	1.58

however, predict radically different liquid ratios in both samples. Mysen (1975) and Bender et al. (1978) have criticized the conclusions of Roeder and Emslie (1970), demonstrating slight temperature and pressure dependencies to the olivine/liquid K_D. No attempt has yet been made to experimentally redetermine orthopyroxene/liquid K_D relations, but it seems improbable that temperature and pressure dependencies of the orthopyroxene K_D would be in the opposite sense to those for olivine. As a result, it must be concluded that the cores of olivine and orthopyroxene phenocrysts in Col 11 and 13 were never in equilibrium, and must have crystallized in two different magmatic environments.

The most probable explanation for the origin of Colima's post-caldera olivine-andesites, therefore, is through the mixing of a basic, olivine-bearing magma with a less basic, orthopyroxene-bearing magma prior to eruption. Titanomagnetites included within olivine phenocrysts of these samples are compositionally distinct from those included within other phases or in the groundmass (Table 16), supporting an independent origin for the olivines. Normally zoned clinopyroxenes, abundant in Col 13, also presumably crystallized in the more basic, end member magma, while the reversely rimmed clinopyroxenes dominating in Col 11 crystallized within the more siliceous, orthopyroxene-bearing magma. Temperatures of 978° and 975° C were calculated from the pyroxene geother-

mometers of Wells (1977) and Wood and Banno (1973) respectively for the average core compositions of the reversely zoned pyroxenes of Col 11. These temperatures are thought to reflect the pre-mixing temperature of the more siliceous end member magma. The values are similar to calculated pyroxene temperatures in Col 9, 6, 17, 18, 2, and 7, implying that the more siliceous end member was a typical, 60%–62% SiO_2 andesite.

Textural and compositional relationships in the plagioclase of Colima's olivine andesites cannot be completely reconciled with the postulated magma mixing origin. As noted by Kuno (1950) for the plagioclase at Hakone Volcano, the included glass in Colima's plagioclase is compositionally indistinguishable from groundmass glass. It is, therefore, unlikely to have formed from closed system heating and recrystallization of the plagioclase. Kuno suggested open system heating involving diffusion between the plagioclase and melt. The plagioclase in Col 11 and 13 is compositionally different from most texturally similar plagioclase discussed in the cited literature in that the clear rims surrounding the glass inclusion riddled core areas are less calcic than the cores. The core plagioclase has not been totally recrystallized to this calcic composition, because phenocrysts with only a penultimate zone of inclusions also have calcic cores. The glass inclusion riddled core areas of Col 11 and 13 plagioclase probably reflect a period of skeletal crystal growth and melt incorporation under supercooled conditions. Supercooling may have resulted from the inferred magma mixing event, but presently unexplained aspects of the scenario include: (1) the location of the plagioclase crystals prior to mixing; high or low temperature end member magma, (2) the cause of the transition from glass inclusion riddled cores to clear rims, and (3) the relative timing of events recorded in plagioclase crystals and those recorded in orthopyroxene crystals. The proposed mixing event presumably induced heterogeneous nucleation of augite on orthopyroxene, resulting in the augite jackets observed in the olivine-andesites. Woodruff and Anderson (1979) observed similar augite jackets in olivine-andesite scoria from a satellite vent of Pavlof Volcano, Alaska. The Pavlof scoria also contain ample evidence of pre-eruptive mixing.

Hornblende-Andesites

Zones of brown glass inclusions in plagioclase phenocrysts and Mg-rich pyroxene rims are also present, though less pronounced, in Colima's post-caldera hornblende-andesites. Slight Mg-rich rims are observed on all orthopyroxenes in pre-1961 hornblende-andesites. As discussed earlier, the post-1961, fourth cycle andesites were probably less hydrous than previous andesites of similar bulk composition which do show Mg-rich pyroxene rims (Col 18, 2, and 7). This observation suggests an alternative to magma mixing as an origin for Mg-rich pyroxene rims.

It must first be assumed that some of the water in Colima's andesites is inherited shortly before eruption. This may occur as groundwater convects into a magma chamber immediately below the volcano, or as hydrothermally altered portions of the volcanic pile are assimilated by the magma. An observation made by Kuno (1950) supports the assumption of a late stage addition of water. In his classic study of Hakone Volcano and its vicinity, Kuno noted that Pliocene volcanics which erupted through a 4-km-thick sequence of marine clastics in the northern part of the region commonly contain hornblende phenocrysts, whereas volcanics erupted to the south, away from this marine basin, are almost devoid of hornblende. Kuno's observation implies that hornblende was stabilized in the northern magmas by a near surface addition of water from the country rock. A similar near surface addition of water may occur at Volcán Colima, and may be responsible for the relatively hydrous nature of its magma system. A detailed study of the oxygen isotopic ratios in andesites from Colima and other Mexican volcanoes is in progress and may ultimately constrain the origin of water in these magmas. As water is added to a magma, its dissociation will cause an increase in magmatic f_{O_2}. This will oxidize a greater amount of the iron in the liquid to Fe^{+3}. In response, all phases will try to reach equilibrium with the lowered Fe^{+2}/Mg ratio of the liquid, and will do so by precipitating relatively Mg-rich rims. This effect will be most pronounced in olivine and orthopyroxene owing to their high MgO contents. In the case of the post-1961, fourth eruptive cycle andesites, it is hypothesized that the near surface addition of water was restricted, resulting in lower magmatic water contents. Consequently, the pyroxenes did not need to precipitate Mg-rich rims in order to remain in equilibrium with the melt. Reverse zoning in pyroxenes may, then, reflect increasing or constant f_{O_2} during crystallization, and not an actual increase in temperature with time.

Plagioclase crystals in Colima's hornblende andesites commonly contain concentric bands of brown glass inclusions. These also probably reflect periods of rapid crystal growth, but the exact cause of this condition is unclear. In a single thin section, some crystals show numerous inclusion bands while others show none at all. It is considered significant that the

percentage of glass inclusions in plagioclase generally correlates with the SiO_2 content of the whole rock samples (Tables 1 and 7). Whatever the cause of the glass inclusions, the effect becomes less obvious in more evolved magmas.

Sequence of Crystallization in the Hornblende-Andesites

In Colima's andesites, plagioclase phenocrysts contain tiny apatite needles, but rarely inclusions of other silicate or oxide phases. Consequently, plagioclase is interpreted as the liquidus silicate phase in each magma. The needle-like morphology of included apatites within both plagioclase and pyroxene phenocrysts, and their common orientation parallel to phenocryst margins suggest that apatite crystallized metastably adjacent to growing crystal faces of other phases and was not itself a stable phase in the magmas. Titanomagnetite inclusions in Colima's pyroxenes are largely restricted to crystal rims, implying that the pyroxenes preceded titanomagnetite in crystallization. In support of this observation, all available experimental data on andesitic systems (Eggler, 1972a; Eggler and Burnham, 1973) demonstrate that titanomagnetite is first stable at least 20° C below the upper temperature of orthopyroxene stability for all realistic values of magmatic f_{O_2} ($\log f_{O_2} = \mathrm{NNO} +/ -1.5$). These experiments also show orthopyroxene to precede clinopyroxene in order of crystallization. Since the inclusion patterns of Colima's orthopyroxenes and clinopyroxenes are indistinguishable, it is concluded that both pyroxenes preceded titanomagnetite. The abundance of titanomagnetite crystals in pyroxene phenocryst rims and their essential absence in plagioclase rims implies a nucleation preference, which may seriously complicate the conventional approach to determining sequences of crystallization from inclusion patterns. Hornblende in Colima's andesites occurs as large crystals which are commonly free of other phases, but do contain titanomagnetite, pyroxene, and plagioclase inclusions. Experimental determination of phase relations in Paricutin and Mt. Hood andesites by Eggler (1972a) and Eggler and Burnham (1973) demonstrate that hornblende is preceded by plagioclase and pyroxenes for all H_2O undersaturated conditions below 5–8 kb confining pressure. Petrographic and experimental observation are consistent, then, with the interpretation that hornblende precipitated last in the crystallization sequence of Colima's andesites, following titanomagnetite. Kuno (1950) reached a similar conclusion regarding the timing of hornblende crystallization in Hakone andesites. Hornblende phenocrysts in Colima's andesites generally have the largest grain size of any phase, despite the fact that they are considered to have crystallized through the smallest temperature interval prior to eruption. This observation demands a high crystal growth rate for hornblende relative to the other phases.

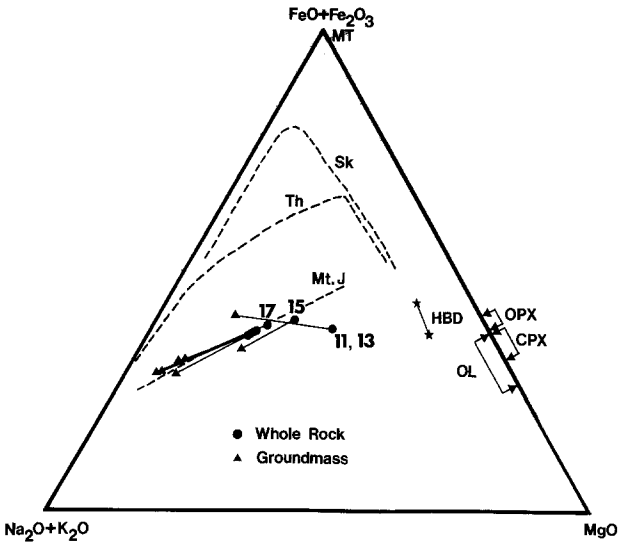

Fig. 9. AFM diagram showing analyzed *whole rock* and *groundmass* points connected by *tie lines*, ranges of phenocryst core compositions, and trends for the tholeiitic Skaergaard (Wager, 1960) and Thingmuli (Carmichael, 1964) suites and the calc-alkaline suite from Mt. Jefferson (McBirney, 1969). wt.%

Compositional Variations Within the Suite

Whole rock and groundmass compositions of analyzed, post-caldera samples are plotted on an AFM diagram in Fig. 9, with each pair joined by a tie line. The compositions of olivine, clinopyroxene, hornblende, and titanomagnetite phenocryst cores in these samples are also indicated, as well as trends for the tholeiitic suites from Skaergaard (Wager, 1960) and Thingmuli (Carmichael, 1964) and the calc-alkaline suite from Mt. Jefferson, a Cascade volcano (McBirney, 1969). Whole rock-groundmass tie lines for the hornblende-andesites are subparallel to one another, to the locus of hornblende-andesite whole rock points, and to the whole rock trend for Mt. Jefferson. The whole rock-groundmass tie line for the olivine-andesite Col 11, has a distinctly different orientation, which simply reflects the presence of olivine rather than hornblende and titanomagnetite as a phenocrystic and microphenocrystic phase.

As seen in Fig. 9, the order of decreasing Fe/Mg in Colima's phenocrystic phases is titanomagnetite – hornblende – orthopyroxene – clinopyroxene – oliv-

ine. Colima's post-caldera andesites display the lack of iron enrichment which is characteristic of calc-alkaline, orogenic suites. If magmas belonging to such a suite are genetically related to one another by crystal-liquid equilibria, such as equilibrium partial melting or crystal fractionation, then a major role must be played by a residual or fractionating mineral with a high Fe/Mg ratio. Candidates that have been suggested for this role include titanomagnetite (Osborn, 1962), hornblende, and garnet (Green and Ringwood, 1968). The data plotted on Fig. 9 qualitatively demonstrate that it is possible to generate Col 15 or 17 from Col 11 through separation of observed olivines and pyroxenes, but that even the analyzed hornblendes are not sufficiently iron-rich to generate the trend of the hornblende-andesites by separation. Garnet is not observed in any of Colima's andesites and is, therefore, untestable in this regard. As noted by Wright (1974) and Barker (1978), normalization procedures employed in the construction of AFM diagrams distort compositional trends, such that crystal fractionation in Colima's magmas can not be quantitatively assessed from Fig. 9. Major element least squares fractionation models (Wright and Doherty, 1970) discussed below allow the derivation of Col 15 from Col 11 by separation of olivine and pyroxenes. Models involving only hornblende + plagioclase separation from Col 15 define a trend slightly displaced from the Col 15-17-9 trend towards the Fe apex. Hornblende fractionation is significantly more effective than pyroxene fractionation in suppressing Fe-enrichment, but exact duplication of the whole rock major element trends from Col 15-9 requires minor coprecipitation of titanomagnetite. Hornblende controlled fractionation also seems unlikely owing to the late position of hornblende in the crystallization sequence of Colima's andesites.

The early progressive enrichment of Fe relative to Mg displayed by tholeiitic suites on AFM diagrams is halted during intermediate stages as titanomagnetite becomes a near liquidus phase driving the trend away from the Fe apex (Carmichael, 1964). Objections to an important role for titanomagnetite in suppressing early Fe-enrichment in calc-alkaline suites have been made on geochemical and experimental grounds. Taylor (1969) argued that separation of sufficient titanomagnetite to inhibit iron enrichment would result in prohibitively low vanadium concentrations in derivative magmas. Since Taylor's study, a number of calc-alkaline suites have been shown to record pronounced decreases in vanadium with increasing silica (Garcia and Jacobson, 1979). Titanomagnetites in analyzed andesites from Volcán Colima contain 2,600–3,600 ppm vanadium. Crystal fractionation models presented in this section involving minor participation by titanomgnetite (0.5–1.0 wt.%), do not encounter severe difficulties in reproducing vanadium contents in Colima's post-caldera suite. Greater difficulties are encountered with other elements, particularly the highly compatible elements Ni and Cr. Experimental arguments against an important role for titanomagnetite fractionation are based on the observation that titanomagnetite is not a near-liquidus phase in calc-alkaline andesites and basalts under realistic f_{O_2} conditions (Eggler, 1972a; Eggler and Burnham, 1973). Petrographic observation of Colima's andesites supports a relatively late (post-pyroxene) position for titanomagnetite in the crystallization sequence. The stability of spinels in calc-alkaline magmas may, however, be significantly enhanced at higher pressures (Garcia and Jacobson, 1979).

Assuming that Colima's post-caldera suite is differentiated by separation of observed phases, titanomagnetite appears to become an important, participating phase by the time magma compositions evolve to that of Col 15 (57% SiO_2). Significant in this regard is the essential absence of phenocrystic and microphenocrystic titanomagnetite in the olivine andesites (0–0.7 vol.%) and its presence in greater amounts (0.8–2.5 vol.%) from Col 15 to more evolved compositions (Table 6).

Realistic geochemical models for the origin of calc-alkaline volcanic suites must be capable of simultaneously treating a variety of processes, including magma mixing and crystal fractionation (O'Hara, 1977). Such complex modeling of an active, dynamic volcanic system is considered beyond the scope of this paper. In this section, we test two very simple end member models for the origin of compositional variations in Colima's post-caldera suite, crystal fractionation and magma mixing.

Crystal Fractionation Models

In order to rigorously test simple crystal fractionation of observed phenocrystic phases as the mechanism producing the observed variations, a two-stage approach was employed (Nelson, 1979). In the first stage, a major element, linear least squares computer program (Wright and Doherty, 1970) was used to calculated the proportions of phases which must be removed from the chosen parent magma in order to derive the chosen daughter magma. P_2O_5, which does not vary significantly through the suite, was not included as a component in the calculations. Analyzed compositions of phenocryst cores in the presumed parent were used in each case. The quality of the fit is indicated by the sum of the squares of the observed minus calculated values for each component

Table 25. Three of the most successful crystal fractionation models assuming total equilibrium for the trace elements (Arth, 1976)

	Col 13 to Col 15			Col 15 to Col 17			Col 17 to Col 9		
	Observed difference	Calculated difference	Residual (r)	Observed difference	Calculated difference	Residual (r)	Observed difference	Calculated difference	Residual (r)
SiO_2	1.38	1.34	0.04	2.58	2.57	0.01	0.56	0.50	0.06
TiO_2	0.02	0.08	−0.06	−0.07	−0.13	0.06	−0.08	−0.06	−0.02
Al_2O_3	0.84	0.82	0.02	−0.34	−0.34	0.00	0.54	0.42	0.12
FeO^t	−0.32	−0.28	−0.04	−0.53	−0.53	0.00	−0.58	−0.64	0.06
MnO	0.00	0.00	0.00	0.00	0.00	0.00	−0.02	−0.01	−0.01
MgO	−1.84	−1.88	0.04	−0.95	−0.95	0.00	−0.47	−0.50	0.03
CaO	−0.60	−0.60	0.00	−1.17	−1.17	0.00	0.03	0.12	−0.10
Na_2O	0.40	0.38	0.02	0.25	0.30	−0.05	0.03	0.12	−0.10
K_2O	0.11	0.14	−0.03	0.24	0.25	−0.01	0.00	0.04	−0.04
	Σr^2:0.01			Σr^2:0.01			Σr^2:0.04		
	Subtracted phases		Wt.% of initial magma	Subtracted phases		Wt.% of initial magma	Subtracted phases		Wt.% of initial magma
	Olivine		3.9	Plagioclase		10.6	Plagioclase		0.1
	Clinopyroxene		4.7	Orthopyroxene		1.2	Orthopyroxene		2.1
	Plagioclase		4.2	Clinopyroxene		1.5	Titanomagnetite		0.5
				Hornblende		7.4			
				Titanomagnetite		0.5			
	% Crystallized		12.8	% Crystallized		21.2	% Crystallized		2.7
	Trace element calculations			Trace element calculations			Trace element calculations		
	low K_D's	high K_D's	Col 15 (Table 2)	low K_D's	high K_D's	Col 17 (Table 2)	low K_D's	high K_D's	Col 9 (Table 2)
Sc	19.4	14.2	18.8 (0.1)	12.3	8.9	14.9 (0.1)[a]	14.5	13.7	12.7 (0.1)[a]
V	248	203	179 (21)	135	82	196 (23)[a]	191	151	150 (25)
Cr	50	15	75 (1)[a]	18	5	35 (1)[a]	18	6	25 (1)[a]
Ni	22	20	51 (8)[a]	33	20	26 (6)	22	17	10 (7)
Zn	53	43	66 (5)[a]	49	37	73 (5)[a]	69	65	70 (4)
Ba	421	414	413 (16)	511	487	497 (17)	510	507	510 (15)
La	10.5	10.4	10.4 (0.5)	12.8	12.5	12.8 (0.5)	13.1	13.0	12.4 (0.5)
Yb	1.89	1.84	1.77 (0.03)[a]	2.00	1.88	1.96 (0.03)	2.00	1.99	1.83 (0.02)[a]
Hf	3.1	3.0	3.1 (0.1)	3.7	3.7	3.8 (0.1)	3.9	3.9	3.5 (0.1)[a]

Numbers in parentheses are counting uncertainties of one standard deviation from INAA (Table 2)

[a] Indicates unsatisfactory fit

(Σr^2). An arbitrary value of $\Sigma r^2 = 1.5$ was chosen as an upper limit of acceptability. As a further simplification, all models calling for the addition of phases to the parent were rejected. Acceptable fractionation models were then subjected to tests involving the trace elements Sc, V, Cr, Ni, Zn, Ba, La, Yb, and Hf as a second stage of the approach. Both surface and total equilibrium conditions were tested (Arth, 1976) using high and low crystal/liquid distribution coefficients listed in Table 18 and the phase proportions calculated from the major element models. A model successfully passed the second test if the concentrations of the nine tested trace elements in the presumed daughter magma fell between the values calculated using the high and low K_D's.

Initially, 71 different models were tested to derive the hornblende-andesites Col 15, 2, 17, 6, and 9 from the olivine-andesite Col 11, and to derive the more siliceous hornblende-andesites from the more basic. 37 of the models passed the major element test, many with excellent fits, but none of these could successfully pass all nine trace element tests under either surface or total equilibrium conditions. Most of the models failed in the prediction of the compatible trace elements (Cr, Ni, and Zn). In each unsuccessful case, the fractionation models predict anomalously low

values for these elements. O'Hara (1977) and Walker (1979) observed that open system fractionation involving simultaneous magma mixing produces precisely this effect, of anomalous enrichment in highly compatible elements. The simple fractionation models considered here are viewed, then, as evidence in support of concurrent magma mixing and crystal fractionation in Colima's magma system. Table 25 lists three of the most successful simple fractionation models for the generation of compositional trends in the sequence Col 13 – Col 15 (1913) – Col 17 (1961) – Col 9 (1975).

Magma Mixing Models

A major element linear least squares program was employed to test the feasibility of forming Col 15, the most basic hornblende-andesite, by mixing Col 11 with Col 17 or 9, and to test the feasibility of forming Col 17, the next most basic hornblende-andesite, by mixing Col 15 with Col 9. All three models were rejected on the basis of Σr^2 values greater than 2. The magma mixing event which is thought to have preceded the eruption of Colima's post-caldera olivine-andesites is discussed further in Part II of this paper. In conclusion, it is not possible to generate all compositional trends observed within the post-caldera suite at Volcán Colima either through simple crystal fractionation or through simple magma mixing using analyzed samples as end members and crystal/liquid trace element distribution coefficients listed in Table 18. Many crystal fractionation models can closely reproduce major element trends of derivative magmas. Even the best of these models, though, fail in the prediction of at least two trace elements. The systematic failure of simple fractionation models to predict sufficient quantities of the compatible trace elements Cr, Ni, and Zn, is taken as evidence that Colima's magma system is periodically injected from below by pulses of relatively primitive magma. In view of the severe restrictions imposed by trace element data on crystal fractionation models, such models which are based solely on major element least squares analysis (Dostal et al., 1977; Fairbrothers et al., 1978) should be viewed with caution.

Summary and Conclusions

Available historical accounts reveal that over the past 400 years, Volcán Colima has evolved through three cycles of eruptive activity, each culminating in a voluminous ashflow eruption. Andesitic block lava eruptions in 1961–1962 and 1975–1976 initiated activity in the fourth historical eruptive cycle which may also terminate with a major ashflow eruption in the early part of the next century. Calculations demonstrate a significant reduction in magmatic water content in the most recent, fourth cycle andesites, however, and this may signal a departure from past behavioral patterns.

Volcán Colima lies closer to the Middle America Trench than any other composite volcano in Mexico. Colima's post-caldera andesites are depleted in K, Ti, *P*, and incompatible trace elements (Zn, Rb, Y, Zr, Ba, La, Yb, Hf, Th, and U) (Luhr and Nelson, 1979), as may be characteristic of near trench andesites. The investigated suite of post-caldera hornblende and olivine-andesites includes products of the four major eruptions since 1869, spanning the two most recent eruptive cycles. From the hornblende-andesite ashflow eruption of 1913, which ended the third eruptive cycle, through the fourth cycle hornblende-andesites, there have been increases in whole rock concentrations of Si, Ba, and Cs, and decreases in Ti, Fe, Mg, Ni, Cr, and Sc. Simple crystal fractionation models can closely reproduce major element variations in the post-caldera suite, but systematically fail to predict sufficient concentrations of the compatible trace elements Cr, Ni, and Zn. O'Hara (1977) and Walker (1979) observed that anomalous enrichments of compatible trace elements result when crystal fractionation is accompanied by periodic mixing with relatively basic magma. Simple magma mixing using compositions of investigated andesites as end-members is not a viable mechanism for producing compositional variations within the post-caldera suite. Analyzed hornblendes in Colima's andesites are too Mg-rich to sufficiently suppress Fe-enrichment in the suite by separation. Small degrees of titanomagnetite separation are required to derive the observed whole rock trend.

Pre-eruptive temperature estimates range from 940°–1,000° C in the hornblende-andesites and 1,030°–1,060° C in the olivine-andesites. Calculated oxygen fugacities lie 1.5 log units above the NNO buffer in T-f_{O_2} space, and calculated pre-eruptive magmatic water contents range from 0.8–3.6 wt.%.

Orthopyroxenes and certain clinopyroxenes in all pre-1961 samples possess relatively Mg-rich rims. The most pronounced Mg-rich rims occur in the olivine-andesites. Analyses of orthopyroxene and olivine phenocryst rim and core compositions in the olivine-andesites indicate pre-eruptive mixing involving andesitic and basaltic end-member magmas. We emphasize that magma mixing is not the only process that can produce relatively Mg-rich rims on mafic phenocrysts. When compared with earlier hornblende-andesites of similar bulk composition, the most recent, fourth cycle andesites display: (1) lower modal hornblende

contents, (2) higher total crystal contents, (3) higher calculated pre-eruptive silica activities, and (4) lower calculated pre-eruptive water contents, in addition to the absence of relatively Mg-rich rims on pyroxenes. All of these features are consistent with the interpretation that the fourth cycle andesites were somewhat less hydrous on eruption. It is suggested that the slightly Mg-rich pyroxene rims in the hornblende-andesites reflect late-stage increases in magmatic water content, which increase magmatic f_{O_2}, and consequently decrease Fe^{+2}/Mg ratios in the melt and all crystalline phases. The fourth cycle andesites apparently did not experience a strong, late-stage influx of water, resulting in lower magmatic water contents and normally zoned pyroxenes.

The abundance of pyroclastic deposits and hornblende-bearing lavas at Volcán Colima and the high f_{O_2} trend of its magmas reflect the relatively hydrous nature of Colima's volcanic system. High water contents may be a primary feature of Colima's near-trench magmas, resulting from vigorous dehydration reactions in the underlying Benioff zone (100 km). Alternatively, the water may be inherited at near surface levels, either as groundwater convects into the volcanic system, or as hydrothermally altered portions of the volcanic pile are assimilated. Slight Mg-rich pyroxene rims in Colima's pre-1961 hornblende-andesites are interpreted as supporting a late stage, high level origin for much of the water in Colima's magmas.

A large body of volcanological and petrographic evidence now exists to support dynamic models for orogenic volcanic system in which crystal fractionation, magma mixing, assimilation of the volcanic pile, and other processes are operating concurrently (Eichelberger, 1975; Anderson, 1976; O'Hara, 1977; Fairbrothers et al., 1978; Johnston, 1978; Yanagi and Ishizaka, 1978; Nelson, 1979; Sakuyama, 1979; Stern, 1979). Recent studies of ocean ridge volcanism increasingly rely on similarly complex models for ridge magma systems (Dungan and Rhodes, 1978; Rhodes et al., 1979; Walker, 1979). Colima's olivine-andesites record petrographic evidence of pre-eruptive magma mixing. In addition, simple crystal fractionation cannot sufficiently enrich derivative magmas in the compatible trace elements Cr, Ni, and Zn. These observations imply that Colima's andesites are also the product of a dynamic subvolcanic magma system, fed from below by pulses of relatively basic magma.

Acknowledgements. We thank S.A. Nelson and C.J. Frisch for assistance in the field, H. Bowman and F. Asaro for NA analyses, and H. Williams for inspiration. Reviews by H. Williams, S.A. Nelson, and A. Ewart significantly improved the manuscript. The support of NSF EAR 74-12782 (Carmichael) is gratefully acknowledged.

References

Allen, J.C., Boettcher, A.L., Marland, G.: Amphiboles in andesite and basalt: I. Stability as a function of P-T-f_{O_2}. Am. Mineral. **60**, 1069–1085 (1975)

Allen, J.C., Boettcher, A.L.: Amphiboles in andesite and basalt: II. Stability as a function of P-T-f_{H_2O}-f_{O_2}. Am. Mineral. **63**, 1074–1087 (1978)

Anderson, A.T.: Magma mixing: Petrological process and volcanological tool. J. Volcanol. Geotherm. Res. **1**, 3–33 (1976)

Anderson, A.T., Clayton, R.N., Mayeda, T.K.: Oxygen isotope thermometry of mafic igneous rocks. J. Geol. **79**, 715–729 (1971)

Ando, S.: Minor element geochemistry of the rocks from Mashu Volcano, Eastern Hokkaido, J. Fac. Sci. Hokkaido Univ. Ser. 4: **16**, No. 4, 553–566 (1975)

Arreola, J.M.: The recent eruptions of Colima. J. Geol. **11**, 749–761 (1903)

Arth, J.G.: Behavior of trace elements during magmatic processes – a summary of theoretical models and their applications. U.S. Geol. Survey, J. Res. **4**, No. 1, 41–47 (1976)

Barcena, M.: Informe Sobre el Estado Actual del Volcan de Colima. pp. 40 Mexico: Imp. Sec. Fomento, 1887

Barker, D.S.: Magmatic trends on alkali-iron-magnesium diagrams. Am. Mineral. **63**, 531–534 (1978)

Bender, J.F., Hodges, F.N., Bence, A.E.: Petrogenesis of basalts from the Project Famous Area: Experimental study from 0 to 15 kbars. Earth Planet. Sci. Lett. **41**, 277–k02 (1978)

Buddington, A.F., Lindsley, D.H.: Iron-titanium oxide minerals and synthetic equivalents. J. Petrol. **5**, 310–357 (1964)

Burnham, C.W., Holloway, J.R., Davis, N.F.: Thermodynamic properties of water to 1000° C and 1000 Bars. Geol. Soc. Am. Spec. Pap. **132**, 1–96 (1969)

Carmichael, I.S.E.: The petrology of Thingmuli, a Tertiary volcano in eastern Iceland. J. Petrol. **5**, part 3, 435–460 (1964)

Carmichael, I.S.E.: The iron-titanium oxides of salic volcanic rocks and their associated ferromagnesian silicates. Contrib. Mineral. Petrol. **14**, 36–64 (1967)

Carmichael, I.S.E., Ghiorso, M.S.: Intensive variables in siliceous magmas. Contrib. Mineral. Petrol. (in press, 1980)

Carmichael, I.S.E., Nicholls, J.: Iron-titanium oxides and oxygen fugacities in volcanic rocks. J. Geophys. Res. **72**, No. 18, 4665–4687 (1967)

Carmichael, I.S.E., Nicholls, J., Spera, F.J., Wood, B.J., Nelson, S.A.: High-temperature properties of silicate liquids: Applications to the equilibration and ascent of basic magma. Philos. Trans. R. Soc. Lond. Ser. A.: **286**, 373–431 (1977)

Condie, K.C., Swenson, D.H.: Compositional variation in three Cascade stratovolcanoes: Jefferson, Ranier, and Shasta, Bull. Volcanol. **37**, No. 2, 205–230 (1973)

Donaldson, C.H., Usselman, T.M., Williams, R.J., Lofgren, G.E.: Experimental modeling of the cooling history of Apollo 12 olivine basalts. Proceeding Lunar Science Conference 6th, 843–869 (1975)

Dostal, J., Capedri, S., De Albuquerque, C.A.R.: Calc-alkaline volcanic rocks from N.W. Sardinia: Evaluation of a fractional crystallization model. Bull. Volcanol. **40**, No. 4, 1–7 (1977)

Drake, M.J.: Plagioclase-melt equilibria. Geochim. Cosmochim. Acta **40**, 457–465 (1975)

Dungan, M.A., Rhodes, J.M.: Residual glasses and melt inclusions in basalts from DSDP Legs 45 and 46: Evidence for magma mixing. Contrib. Mineral. Petrol. **67**, 417–431 (1978)

Eggler, D.H.: Water-saturated and undersaturated melting relations in a Paricutin andesite and an estimate of water content in the natural magma. Contrib. Mineral. Petrol. **34**, 261–271 (1972a)

Eggler, D.H.: Amphibole stability in H_2O-undersaturated calc-alkaline melts. Earth Planet. Sci. Lett. **15**, 28–34 (1972b)

Eggler, D.H., Brurnham, C.W.: Crystallization and fractionation trends in the system andesite $-H_2O-CO_2-O_2$ at pressures to 10 Kb. Geol. Soc. Am. Bull. **84**, 2517–2532 (1973)

Eichelberger, J.C.: Origin of andesite and dacite: Evidence of mixing at Glass Mountain in California and at other circum-Pacific volcanoes. Geol. Soc. Am. Bull. **86**, 1381–1391 (1975)

Eichelberger, J.C.: Andesitic volcanism and crustal evolution. Nature 275, No. 7, 21–27 (1978)

Evans, S.H. Jr., Nash, W.P.: Petrogenesis of xenolith-bearing basalts from southeastern Arizona. Am. Mineral. **64**, 249–267 (1979)

Ewart, A., Hildreth, W., Carmichael, I.S.E.: Quaternary acid magma in New Zealand. Contrib. Mineral. Petrol. **51**, 1–27 (1975)

Fairbrothers, G.E., Carr, M.J., Mayfield, D.G.: Temporal magmatic variation at Boqueron Volcano, El Salvador. Contrib. Mineral. Petrol. **67**, 1–9 (1978)

Flowers, G.C.: Correction of Holloway's (1977) adaptation of the Modified Redlich-Kwong equation of state for calculation of the fugacities of molecular species in supercritical fluids of geologic interest. Contrib. Mineral. Petrol. **69**, 315–318 (1979)

Foshag, W.F., Gonzalez, R.J.: Birth and development of Paricutin Volcano, Mexico, U.S. Geol. Surv. Bull. **965**-D, 355–489 (1956)

Francis, P.W., Robool, M.J., Walker, G.P.L., Cobbold, P.R., Coward, M.: The San Pedro and San Pablo Volcanoes of northern Chile and their hot avalanche deposits. Geol. Rundsch. **63**, 357–388 (1974)

Friedlaender, I.: Über die Mexikanischen Vulkane Pico de Orizabo, Cerro de Tequila, und Colima. Z. Vulkanol. **13**, 154–164 (1930)

Fudali, R.F.: Oxygen fugacities of basaltic and andesitic magmas: Geochim. Cosmochim. Acta **29**, 1063–1075 (1965)

Garcia, M.O., Jacobson, S.S.: Crystal clots, amphibole fractionation, and the evolution of calc-alkaline magmas. Contrib. Mineral. Petrol. **69**, No. 4, 319–332 (1979)

Gastil, R.G., Jensky, W.: Evidence for strike-slip displacement beneath the Trans-Mexican Volcanic Belt. Stanford University Published in Geol. Sci. 12–13, 171–180 (1973)

Ghiorso, M.S., Carmichael, I.S.E.: A regular solution model for met-aluminous silicate liquids: Applications to geothermometry, liquid immiscibility, and the source regions of basic magmas. Contrib. Mineral. Petrol. (in press, 1979)

Green, T.H., Ringwood, A.E.: Genesis of the calc-alkaline igneous rock suite. Contrib. Mineral. Petrol. **18**, 105–162 (1968)

Gutmann, J.T.: Textures and genesis of phenocrysts and megacrysts in basaltic lavas from the Pinacate volcanic field. Am. J. Sci. **277**, 833–861 (1977)

Hatherton, T., Dickenson, W.R.: The relationship between andesitic volcanism and seismicity in Indonesia, the Lesser Antilles, and other island arcs. J. Geophys. Res. **74**, 5301–5310 (1969)

Helgeson, H.C., Delany, J.M., Nesbitt, H.W., Bird, D.K.: Summary and critique of the thermodynamic properties of rock forming minerals. Am. J. Sci. **278A**, 220 pp. (1978)

Helz, R.T.: Phase relations of basalts in their melting range at $P_{H_2O} = 5$ Kb as a function of oxygen fugacity: Part I. Mafic phases. J. Petrol. **14**, part 2, 249–302 (1973)

Jakes, P., White, A.J.R.: Major and trace element abundances in volcanic rocks of orogenic areas. Geol. Soc. Am. Bull. **83**, 29–40 (1972)

Johnston, D.A.: Volatiles, magma mixing, and the mechanism of eruption of Augustine Volcano, Alaska. University of Washington, Unpublished Ph. D. dissert, 177 p. 1978

Katsui, Y., Ando, S., Inaba, K.: Formation and magmatic evolution of Mashu Volcano, East Hokkaido, Japan. J. Fac. Sci. Hokkaido Univ. Ser. 4: **16**, No. 4, 533–552 (1975)

Katsui, Y., Oba, Y., Ando, S., Nishimura, S., Masuda, Y., Kurasawa, H., Fujimaki, H.: Petrochemistry of the Quaternary volcanic rocks of Hokkaido, North Japan. J. Fac. Sci. Hokkaido Univ. Ser. 4: **18**, No. 3, 449–484 (1978)

Kudo, A.M., Weill, D.F.: An igneous plagioclase geothermometer. Contrib. Mineral. Petrol. **25**, 52–65 (1970)

Kuno, H.: Petrological notes on some pyroxene-andesites from Hakone Volcano, with special reference to some types with pigeonite phenocrysts. Jpn. J. Geol. and Geogr. **13**, 107–140 (1936)

Kuno, H.: Petrology of Hakone Volcano and the adjacent areas, Japan. Geol. Soc. Am. Bull. **61**, 957–1020 (1950)

Kuno, H.: Origin of Cenozoic petrographic provinces of Japan and surrounding areas. Bull. Volcanol. **20**, 37–76 (1959)

Kyser, T.K., O'Neil, J.R., Carmichael, I.S.E.: Oxygen isotope fractionations between coexisting phases at high temperatures and their bearing on the genesis of basic lavas and mantle xenoliths. Submitted for publication (1980)

Lofgren, G.E., Donaldson, C.H., Williams, R.J., Mullins, O. Jr., Usselman, T.M.: Experimentally reproduced textures and mineral chemistry of Apollo 15 quartz-normative basalts. Proc. Lunar Sci. Conf. 5th, 549–567, 1974

Lofgren, G.E., Usselman, T.M.: Geology, petrology, and crystallization of Apollo 15 quartz-normative basalts. Proc. Lunar Sci. Conf. 6th, 79–99, 1975

Lorenzo, J.L.: Notas Sobre Geologia Glacial del Nevado de Colima. Boletin del Instituto de Geologia, Univ. Natl. Auton. Mexico **61**, 77–92 (1961)

Luhr, J., Carmichael, I.S.E.: Basanite and minette cinder cones from the northern flanks of the andesitic Colima volcanoes, Mexico. Geol. Soc. Am. Abstr. Prog. **11**, No. 7, 469–470 (1979)

Luhr, J., Nelson, S.A.: Volcanological and geochemical contrasts between two Mexican volcanoes: Colima and Ceboruco. EOS, Trans. Am. Geophys. Union, 1979 PNW Meeting, abstracts (1979)

MacDonald, G.A. Katsura, T.: Eruption of Lassen Peak, Cascade Range, California, in 1915: Example of mixed magmas. Geol. Soc. Am. Bull. **76**, 475–482 (1965)

Mahood, G.A.: A preliminary report on the comenditic dome and ashflow complex of Sierra La Primavera, Jalisco. Univ. Nal. Auton. Mexico, Inst. Geologia, Revista **1**, No. 2, 177–190 (1977)

Marsh, B.D.: Some Aleutian andesites: Their nature and source. J. Geol. **84**, 27–45 (1976)

McBirney, A.R.: Petrochemistry of the Cascade andesite volcanoes. Oregon Dept. of Geol. and Mineral. Ind. **65**, 101–107 (1969)

Medaris, L.G., Jr.: Partitioning of Fe^{2+} and Mg^{2+} between coexisting synthetic olivine and orthopyroxene. Am. J. Sci. **267**, 945–968 (1969)

Molnar, P., Sykes, L.R.: Tectonics of the Caribbean and Middle America regions from focal mechanisms and seismicity. Geol. Soc. Am. Bull. **80**, 1639–1684 (1969)

Moorbath, S., Thorpe, R.S., Gibson, I.L.: Strontium isotope evidence for petrogenesis of Mexican andesites. Nature **271**, 437–439 (1978)

Mooser, F.: Active volcanoes of Mexico: International Volc. Assn. Catalogue of Active Volcanoes, part VI, 1958

Mooser, F.: Los Volcanes de Colima. Universidad Nacional, Mexico, Geol. Bol. **61**, 49–71 (1961)

Mooser, F.: The Mexican Volcanic Belt – Structure and development. Formation of fractures by differential crustal heating, Pan American Symp. on the Upper Mantle, Mexico, 15–222, 1969

Mooser, F.: The Mexican Volcanic Belt: Structure and tectonics. Geofis. Int. **12**, 55–70 (1972)

Mooser, F., Maldonando-Koerdell, M.: State of the volcanoes – Colima Volcano, renewed activity. Mexican National Report

on Volcanology, XI[th] General Assembly of the I.U.G.G., Extrait du Bull. Volcanol. ser. **2**, Tome 21, 164 (1959)
Mooser, F., Maldonando-Koerdell, M.: State of the volcanoes – Colima Volcano. Mexican National Report on Volcanology, XIII[th] General Assembly of the I.U.G.G., 1963
Mysen, B.: Partitioning of iron and magnesium between crystals and partial melts in peridotite upper mantle. Contrib. Mineral. Petrol. **52**, 69–76 (1975)
Nakamura, Y.: Geology and petrology of Bandai and Nekoma volcanoes. Sci. Rep. Tohoku Univ. Ser. 3, 14, No. 1, 67–119 (1978)
Nelson, S.A.: The geology and petrology of Volcán Ceboruco, Nayarit, Mexico. University of California, Berkeley, Unpublished Ph. D. dissert., Part I, 164 p. 1979
Newhall, C.G.: Temporal variation in the lavas of Mayon Volcano, Philippines. Geol. Soc. Am. Abstr. Prog. **10**, No. 3, 139 (1978)
O'Hara, M.J.: Geochemical evolution during fractional crystallization of a periodically refilled magma chamber. Nature **266**, No. 7, 503–507 (1977)
Osborn, E.F.: Reaction series for subalkaline igneous rocks based on different oxygen pressure conditions. Am. Mineral. **47**, 211–226 (1962)
Peacock, M.A.: Classification of igneous rock series. J. Geol. **39**, 54–67 (1931)
Perlman, I., Asaro, F.: Pottery analysis by neutron activation. Archaeometry **11**, 21–52 (1969)
Pichler, H., Weyl, R.: Quaternary alkaline rocks in eastern Mexico and Central America. Munster. Forsch. Geol. Palaont. **38–39**, 159–178 (1976)
Powell, R.: Thermodynamics of coexisting cummingtonite-hornblende pairs. Contrib. Mineral. Petrol. **51**, 29–37 (1975)
Rhodes, J.M., Dungan, M.A., Blanchard, D.P., Long, P.E.: Magma mixing at mid-ocean ridges: Evidence from basalts drilled near 22° N on the Mid-Atlantic ridge. Tectonophysics **55**, 35–61 (1979)
Rittmann, A.: Volcanoes and their activity: Trans. of 2[nd] German Edition by E.A. Vincent, INTERSCIENCE Publ., New York. 305 pp. (1962)
Robin, C., Tournon, J.: Spatial relations of andesitic and alkaline provinces in Mexico and Central America. Can. J. Earth Sci. **15**, 1633–1641 (1978)
Roeder, P.L., Emslie, R.F.: Olivine-liquid equilibrium. Contrib. Mineral. Petrol. **29**, 275–289 (1970)
Rose, W.I., Jr., Grant, N.K., Hahn, G.A., Lange, I.M., Powell, J.L., Easter, J., DeGraff, J.M.: The evolution of Santa Maria Volcano, Guatemala. J. Geol. **85**, 63–87 (1977)
Sakuyama, M.: Evidence of magma mixing: Petrological study of Shirouma-Oike calc-alkaline andesite volcano, Jpn. J. Volcanol. Geotherm. Res. **5**, 179–208 (1979)
Sapper, K.: VULKANKUNDE. pp. 424 J. Engelhorns Nachf. Stuttgart: 1927
Sartorius, C.: Eruption of the volcano of Colima in June, 1869. Am. J. Sci. **102**, 381–383 (1871)
Sperry, F.L.: The eruption of Colima. Am. J. Sci. **15**, 487–488 (1903)
Stern, C.R., Huang, W., Wyllie, P.J.: Basalt-andesite-rhyolite-H_2O: Crystallization intervals with excess H_2O and H_2O-undersaturated liquidus surfaces to 35 kbars, with implications for magma genesis. Earth Planet. Sci. Lett. **28**, 189–196 (1975)
Stern, R.J.: On the origin of andesite in the Northern Mariana Island Arc: Implications from Agrigan. Contrib. Mineral. Petrol. **68**, No. 2, 207–219 (1979)
Stewart, D.C.: Crystal clots in calc-alkaline andesites as breakdown products of high-Al amphiboles. Contrib. Mineral. Petrol. **53**, 195–204 (1975)
Stoiber, R.E.: Products of the fumaroles, Colima Volcano, Mexico. Yearb. Am. Philos. Soc. 295–297 (1967)
Stormer, J.C., Jr., Carmichael, I.S.E.: The Kudo-Weill plagioclase geothermometer and porphyritic acid glasses. Contrib. Mineral. Petrol. **28**, 306–309 (1970)
Sugimura, A.: Spatial relations of basaltic magmas in island arcs. In: *Treatise on Basalts*. (H.H. Hess and A. Poldervaart eds.), pp. 537–572. Vol. 2. INTERSCIENCE, New York (1968)
Taylor, S.R.: Trace element chemistry of andesites and associated calcalkaline rocks. Oregon Dept. Geol. and Miner. Ind. Bull. **65**, 43–63 (1969)
Thorpe, R.S.: Tectonic significance of alkaline volcanism in eastern Mexico. Tectonophysics **40**, 19–26 (1977)
Thorpe, R.S., Gibson, I.L., Vizcaino, J.S.: Andesitic pyroclastic flows from Volcán Colima. Nature **265**, 724–725 (1977)
Ulmer, G.C., Rosenhauer, M., Woermann, E., Ginder, J., Drory-Wolff, A., Wasilewski, P.: Applicability of electrochemical oxygen fugacity measurements to geothermometry. Am. Mineral. **61**, 653–660 (1976)
Wager, L.R.: The major element variation of the layered series of the Skaergaard intrusion and a re-estimation of the average composition of the hidden layered series and of the successive residual magmas. J. Petrol. **1**, 364–398 (1960)
Walker, D.: Phase equilibrium curvature effects on mixed magma. EOS. Trans. Am. Geophys. Union, 1979 PNW Meeting, abstr., 1979
Waitz, P.: Le Volcan de Colima. 10[th] International Geological Congress, Field Trip Guide, chap. 13, p. 27, 1906
Waitz, P.: Der Gegenwärtige Zustand der Mexikanischen Vulkane und die Letzte Eruption des Vulkans von Colima (1913). Z. Vulkanol. **1**, 247 (1915)
Waitz, P.: Datos historicos y bibliograficos arcerca del Volcán de Colima. In: Mem. Soc. Cient (Antonio Alzate, ed.), Vol. **53**, pp. 349–384 Mexico: Tomo 1932
Wells, P.R.A.: Pyroxene thermometry in simple and complex systems. Contrib. Mineral. Petrol. **62**, 129–139 (1977)
Weyl, R.: Vulkanismus und Vulkanlandschaft im Hochland von Mexiko. Nat. Mus. **104**, No. 5, 137–152 (1974)
White, S.E.: A geologic investigation of the late Pleistocene histroy of the volcano Popocatepetl, Mexico. Syracuse University, Unpublished Ph. D. dissert., 350 p. 1952
Wilcox, R.E.: Petrology of Paricutin Volcano, Mexico. U.S. Geol. Surv. Bull. **965-C**, 281–349 (1954)
Williams, H.: Volcanoes of the Paricutin Region. U.S. Geol. Surv. Bull. **965-D**, 165–275 (1950)
Williams, R.J., Eugster, H.P.: An experimental study of (Fe, Mg), olivine – (Fe, Mg) pyroxene reactions and their geological applications. Geol. Soc. Am. Abstr. Prog. **237**, (1969)
Wood, B.J., Banno, S.: Garnet-orthopyroxene and orthopyroxene-clinopyroxene relationships in simple and complex systems. Contrib. Mineral. Petrol. **42**, 109–124 (1973)
Woodruff, L.G., Anderson, A.T.: An arrested state of magma mixing, Pavlof Volcano, Alaska: EOS, Trans. Am. Geophys. Union, 1979 PNW Meeting, abstr. 1979
Wright, T.L.: Presentation and interpretation of chemical data for igneous rocks. Contrib. Mineral. Petrol. **48**, 233–248 (1974)
Wright, T.L., Doherty, P.C.: A linear programming and least squares computer method for solving petrologic mixing problems. Geol. Soc. Am. Bull. **81**, 1995–2008 (1970)
Wright, T.L., Weiblen, P.W.: Mineral compositions and paragenesis in tholeiitic basalt from Makuopuhi lava lake, Hawaii. Geol. Soc. Am. Spec. Pap. **115**, 242–243 (1968)
Yanugi, T., Ishizaka, K.: Batch fractionation model for the evolution of volcanic rocks in an island arc: An example from central Japan. Earth Planet. Sci. Lett. **40**, 252–262 (1978)

Received September 5, 1979; Accepted November 1, 1979